



The Complete Classification of Solutions to the Riemann Problem of the Defocusing Complex Modified KdV Equation

Deng-Shan Wang¹ · Ling Xu² · Zuxing Xuan³

Received: 27 February 2021 / Accepted: 25 October 2021 / Published online: 25 November 2021
© The Author(s), under exclusive licence to Springer Science+Business Media, LLC, part of Springer Nature 2021

Abstract

The complete classification of solutions to the defocusing complex modified KdV equation with step-like initial condition is studied by the finite-gap integration approach and Whitham modulation theory. All kinds of combination solutions consisting of genus-0 regions, genus-1 regions, or genus-2 regions are found by classifying the Riemann invariants. The behaviors of wave breaking in Riemann problem of the defocusing complex modified KdV equation are much richer and more complicated than those in the nonlinear Schrödinger equation. It is demonstrated that a large oscillating region can be composed of four basic genus-1 dispersive shock waves, a case of solution may be consisted of up to six regions, and the plateau, vacuum, rarefaction wave, and dispersive shock wave can coexist in the same solution region. Moreover, the genus-2 region, produced from the collision of two dispersive shock waves, is described detailedly by the genus-2 Whitham equations. The direct numerical simulations on the defocusing complex modified KdV equation show remarkable agreement with the results from Whitham modulation theory.

Keywords Complex modified KdV equation · Whitham equations · Rarefaction wave · Dispersive shock wave · Riemann invariant · Whitham modulation theory

Mathematics Subject Classification 37K10 · 35J10 · 76L05

Communicated by Peter Miller.

✉ Deng-Shan Wang
dswang@bnu.edu.cn

¹ Laboratory of Mathematics and Complex Systems (Ministry of Education), School of Mathematical Sciences, Beijing Normal University, Beijing 100875, People's Republic of China

² School of Applied Science, Beijing Information Science and Technology University, Beijing 100192, People's Republic of China

³ Institute of Fundamental and Interdisciplinary Sciences, Beijing Union University, Beijing 100101, People's Republic of China

1 Introduction

The Whitham theory was first formulated by G.B. Whitham in his seminal publication (Whitham 1965) in which he gave the Whitham modulation equations based on the averaged conservation laws to describe some physical phenomena such as undular bore in water and formed the basis of impressive development of dispersive hydrodynamics. The first application of Whitham theory to Korteweg–de Vries (KdV) equation was achieved by Gurevich and Pitaevskii (1974) who studied the self-similar solutions for dispersive shock wave (DSW), called collisionless shock, whose evolution can be described by the diagonal Whitham equation. One of its edge appears to be a soliton wave, the harmonic wave for its opposite. The simplest expanding oscillating structure described by a Jacobian elliptic function was also obtained in Gurevich and Pitaevskii (1974) with a step-like initial jump known as Riemann problem. The analytical description of DSW that transformed the Whitham equation to Euler–Poisson–Darboux equation for the nonlinear Schrödinger equation (NLS) has been presented in Tian and Ye (1999).

The Riemann problem of the evolution waves has been discussed in various important physical fields. In photon fluid, all the possible wave patterns propagating in the normal fiber has been discussed with account of steepening effects (Ivanov and Kamchatnov 2017). Ivanov et al. (2017) gives the classification of possible flows in two-component Bose–Einstein condensate and the solutions of Riemann problem for Gardner equation (related to modified KdV equation) are completely classified in Kamchatnov et al. (2012) which appears some new structures and more complicated cases compared to the KdV case. Indeed, this can also be found in the case of defocusing complex modified KdV (cmKdV) equation with special step-like initial data (Kodama et al. 2008; Kong et al. 2019). However, the studies on general step-like initial problem of the defocusing cmKdV equation are even more complicated.

Except the pseudo-phase method introduced by Whitham himself, there are several way to average the original equation to get the Whitham equations. For example, Luke (1966) used a perturbation procedure to investigate the nonlinear wave problem, which could recover the Whitham equations of slow variations. Flaschka et al. (1980) extended the finite-gap integration theory to study the multiphase averaging of integrable system of KdV type. Dubrovin and Novikov (1989) proposed a procedure for averaging the local Poisson brackets to derive the Whitham equations. Lax and Levermore (1983) opened another way to describe the DSW rigorously by utilizing the method of inverse scattering transform and Whitham modulation theory. Moreover, the combinations of Whitham modulation theory with numerical techniques have been studied by Grava and Klein (2007) and Ablowitz et al. (2016).

This paper focuses on the complete classification of Riemann problem for the defocusing cmKdV equation with small dispersion

$$q_t - 6|q|^2 q_x + \varepsilon^2 q_{xxx} = 0, \quad (1)$$

where $q = q(x, t)$ represents the complex wave envelope and $\varepsilon \ll 1$ is a small modulation scale. This equation is analyzed by means of Whitham modulation theory, in which the corresponding Whitham equations are neither strictly hyperbolic nor

genuinely elliptic systems (Kodama et al. 2008) compared with the defocusing and focusing NLS equations. Self-similar solutions in such kind of systems have been investigated and discussed in KdV hierarchy (Pierce and Tian 2007), mKdV (Kamchatnov et al. 2012), Landau–Lipshitz equation (Ivanov et al. 2017), Camassa–Holm equation (Abenda and Grava 2005), etc. However, it is found in this work that the solutions in the defocusing cmKdV equation are much richer such as an oscillating shock wave region may be composed of four basic shock wave structures and a case of solution can be consisted of up to six regions, etc. In addition, the whole solutions we have classified are even more than 50 categories, which has never been found before.

The Madelung transformation

$$q(x, t) = \sqrt{\rho} e^{i\phi/\varepsilon}, \quad \phi_x = v, \quad (2)$$

where ρ and v , analogs of density and velocity of the hydrodynamics, are all real functions, maps the defocusing cmKdV equation (1) to the dispersive hydrodynamics-like system

$$\begin{cases} \rho_t - (3\rho^2 + 3v^2\rho)_x = -\varepsilon^2(4\rho^{3/4}(\rho^{1/4})_{xx})_x, \\ v_t - (6\rho v + v^3)_x = -\varepsilon^2(3v\rho_{xx}/2\rho - 3v(\rho_x)^2/4\rho^2 + 3v_x\rho_x/2\rho + v_{xx})_x, \end{cases} \quad (3)$$

which suffice to give the solutions as $\varepsilon \rightarrow 0$ until it develops a shock formed at once when multi-value region appears. After the moment when multi-value region appears, this limit is converted into the Whitham equations in the diagonal Riemann form Grava and Klein (2007), Ablowitz et al. (2016), Pierce and Tian (2007), Abenda and Grava (2005), Hoefer (2014), Ivanov and Kamchatnov (2017), Ablowitz et al. (2020), Bridges and Ratliff (2021) and Congy et al. (2019)

$$\frac{\partial \lambda_i}{\partial t} + v_i(\lambda_1, \lambda_2, \dots, \lambda_{2N+2}) \frac{\partial \lambda_i}{\partial x} = 0, \quad i = 1, 2, \dots, 2N + 2, \quad (4)$$

where v_i are called the Whitham velocities, λ_i are Riemann invariants and N represents the number of phases in the oscillations. The boundaries connecting $N = 0$ and $N = 1$ regions including in Whitham equations (4) are exactly the same with the diagonal Riemann form of dispersionless limit of hydrodynamics-like system (3), which will be explained below. Here we concentrate only on the case of $0 \leq N \leq 2$, while the case $N > 2$ will be discussed in the future work.

This paper is constructed as follows. In Sect. 2, the zero-phase, one-phase and two-phase periodic solutions and the corresponding Whitham equations are derived by employing the finite-gap integration approach. In Sect. 3, five types of basic rarefaction wave structures and ten types of basic dispersive shock wave structures are proposed by considering the self-similar solutions of the Whitham equations. The complete classification of solutions to the Riemann problem of the defocusing cmKdV equation (1) is investigated analytically and numerically in Sect. 4. We conclude this work in Sect. 5.

2 Finite-Gap Periodic Solutions and Whitham Equations

In this section, the finite-gap periodic solutions and Whitham equations for the defocusing cmKdV equation (1) are derived by the Flaschka–Forest–McLaughlin (FFM) approach (Flaschka et al. 1980; Kamchatnov 1994, 1997) to describe its evolutions of initial discontinuities in Riemann problem. For our purpose, this section only focuses on the zero-phase, one-phase, and two-phase solutions in view of the form of the step-like initial data considered in this work.

It is known that the defocusing cmKdV equation (1) is the second flow in the defocusing NLS hierarchy, which has Lax pair of the form

$$\varepsilon \begin{pmatrix} \psi_1 \\ \psi_2 \end{pmatrix}_x = \begin{pmatrix} F & G \\ H & -F \end{pmatrix} \begin{pmatrix} \psi_1 \\ \psi_2 \end{pmatrix}, \quad \varepsilon \begin{pmatrix} \psi_1 \\ \psi_2 \end{pmatrix}_t = \begin{pmatrix} A & B \\ C & -A \end{pmatrix} \begin{pmatrix} \psi_1 \\ \psi_2 \end{pmatrix}, \quad (5)$$

where the entries of the matrices above are

$$\begin{aligned} F &= -i\lambda, & G &= q, & H &= q^*, & A &= -4i\lambda^3 - 2i\lambda|q|^2 - \varepsilon q q_x^* + \varepsilon q^* q_x, \\ B &= 4\lambda^2 q + 2i\lambda \varepsilon q_x + 2q|q|^2 - \varepsilon^2 q_{xx}, & C &= 4\lambda^2 q^* - 2i\lambda \varepsilon q_x^* + 2q^*|q|^2 - \varepsilon^2 q_{xx}^*. \end{aligned} \quad (6)$$

The linear systems (5) and (6) have two independent basic solutions (ψ_1, ψ_2) and (ϕ_1, ϕ_2) , which can be used to define the “squared” eigenfunctions as follows

$$f = -\frac{i}{2}(\psi_1\phi_2 + \psi_2\phi_1), \quad g = \psi_1\phi_1, \quad h = -\psi_2\phi_2, \quad (7)$$

which dates back to the work of Its and Kotlyarov Kotlyarov (1976), Its and Kotlyarov (1976). Obviously, the “squared” eigenfunctions f, g and h satisfy the following linear systems

$$\varepsilon f_x = -iHg + iGh, \quad \varepsilon g_x = 2iGf + 2Fg, \quad \varepsilon h_x = -2iHf - 2Fh, \quad (8)$$

and

$$\varepsilon f_t = -iCg + iBh, \quad \varepsilon g_t = 2iBf + 2Ag, \quad \varepsilon h_t = -2iCf - 2Ah. \quad (9)$$

In fact, the linear systems (8) and (9) compose a three-order Lax pair of the defocusing cmKdV equation (1). Further, it is convenient to prove that the quantity $f^2 - gh = (-1/4)(\psi_1\phi_2 - \psi_2\phi_1)^2$ is independent of x and t , and is only dependent on the spectral parameter λ , which can be denoted by

$$f^2 - gh = P(\lambda), \quad (10)$$

where $P(\lambda)$ is polynomial of parameter λ .

One merit of the linear systems (8) and (9) is that they can be used to derive the conservation laws of the defocusing cmKdV equation (1). Indeed, the second equations

in both equation (8) and (9) can be rewritten as

$$\varepsilon(\log(g))_x = \varepsilon \frac{g_x}{g} = 2if \frac{G}{g} + 2F, \quad \varepsilon(\log(g))_t = \varepsilon \frac{g_t}{g} = 2if \frac{B}{g} + 2A. \tag{11}$$

The compatibility condition of these two equations indicates that

$$\frac{\partial}{\partial t} \left(2if \frac{G}{g} + 2F \right) = \frac{\partial}{\partial x} \left(2if \frac{B}{g} + 2A \right), \tag{12}$$

which can be simplified to

$$\frac{\partial}{\partial t} \left(\frac{G}{g} \right) - \frac{\partial}{\partial x} \left(\frac{B}{g} \right) = 0. \tag{13}$$

This is just the conservation law of the defocusing cmKdV equation (1) in term of the “squared” eigenfunction g .

For the AKNS system like the defocusing cmKdV equation (1), it is convenient to expand f , g and h to finite-order polynomials in λ

$$f(x, t, \lambda) = \sum_{j=0}^{N+1} f_j(x, t)\lambda^j, \quad g(x, t, \lambda) = \sum_{j=0}^{N+1} g_j(x, t)\lambda^j, \quad h(x, t, \lambda) = \sum_{j=0}^{N+1} h_j(x, t)\lambda^j. \tag{14}$$

The second and third equations in Eq. (8) show that both g and h must be of order N in λ (i.e., $g_{N+1} = h_{N+1} = 0$), thus the first equation in Eq. (8) indicates that the coefficient f_{N+1} of λ^{N+1} is a constant. Without any loss of generality, one can set $f_{N+1} = 1$. In order to derive the N -phase solution, assume

$$g(x, t, \lambda) = q \prod_{j=1}^N (\lambda - \mu_j(x, t)), \tag{15}$$

where $\mu_j = \mu_j(x, t)$ is called auxiliary spectrum, N is the genus of the hyperelliptic curve

$$w^2 = P(\lambda). \tag{16}$$

Plugging Eq. (15) into Eqs. (8) and (9) and letting $\lambda = \mu_k(x, t)$ ($k = 1, 2, \dots, N$), yield Dubrovin-type equation for $\mu_k(x, t)$ as

$$\begin{aligned} \varepsilon \frac{\partial \mu_k}{\partial x} &= - \frac{2i \tilde{G} \sqrt{P(\mu_k)}}{\prod_{j \neq k} (\mu_k - \mu_j)}, \\ \varepsilon \frac{\partial \mu_k}{\partial t} &= - \frac{2i \tilde{B} \sqrt{P(\mu_k)}}{\prod_{j \neq k} (\mu_k - \mu_j)}, \quad j = 1, 2, \dots, N, \end{aligned} \tag{17}$$

where $\tilde{G}(\mu_k) = G(\mu_k)/q = 1$, $\tilde{B}(\mu_k) = B(\mu_k)/q = 4\mu_k^2 + 2i\varepsilon\mu_k(\ln q)_x + 2|q|^2 - \varepsilon^2 q_{xx}/q$.

Substituting Eq. (14) with Eq. (15) into the second equation in Eqs. (8) and (9), respectively, yields

$$\begin{aligned} \epsilon q_x &= 2iq \left(f_N + \sum_{j=1}^N \mu_j \right), \\ \epsilon q_t &= 2i[4qf_{N-2} + 2i\epsilon q_x f_{N-1} + f_N(2q|q|^2 - \epsilon^2 q_{xx})] \\ &\quad + 2 \left[q(\epsilon q^* q_x - \epsilon q q_x^*) + 4iq \sum_{i < j < k} \mu_i \mu_j \mu_k + 2i|q|^2 \sum_{j=1}^N \mu_j \right]. \end{aligned} \tag{18}$$

An algebro-geometric representation of $q(x, t)$ in Eq. (18) can be developed by integrating the Dubrovin-type equation (17) for μ_k ($k = 1, 2, \dots, N$) with the aid of the Abel transform, which leads to the expressions for μ_k and $q(x, t)$ in terms of Riemann theta functions depending on phase variables

$$\theta_j = \kappa_j x + \omega_j t + \theta_{0j}, \quad j = 1, 2, \dots, N, \tag{19}$$

where κ_j and ω_j are determined by integrating over certain cycles on the Riemann surface of the hyperelliptic curve (16), and θ_{0j} are constants.

In the framework of Whitham theory, it is vital to derive the Whitham equations of Riemann invariants, which are the zero points λ_i ($i = 1, 2, \dots, 2N + 2$) of the polynomial $P(\lambda)$ in Eq. (10). The FFM approach (Flaschka et al. 1980) for studying Whitham equations is based on the finite-gap integration theory, which is an important extension of the inverse scattering transform to the problems of periodic boundary conditions (Belokolos et al. 1994). The construction of multiphase averaging in FFM way is further extended by Kamchatnov (1994, 1997) without use of algebro-geometric tools like FFM approach. We now outline the basic procedure for deriving the Whitham equations of the defocusing cmKdV equation (1).

Firstly, normalizing the equation $f^2 - gh = P(\lambda)$ according to the transformation $f \rightarrow f/\sqrt{P(\lambda)}$, $g \rightarrow g/\sqrt{P(\lambda)}$ and $h \rightarrow h/\sqrt{P(\lambda)}$ yields

$$\left(f/\sqrt{P(\lambda)} \right)^2 - \left(g/\sqrt{P(\lambda)} \right) \left(h/\sqrt{P(\lambda)} \right) = 1.$$

Under the same transformation, the conservation law (13) becomes

$$\frac{\partial}{\partial t} \left(\frac{G\sqrt{P(\lambda)}}{g} \right) - \frac{\partial}{\partial x} \left(\frac{B\sqrt{P(\lambda)}}{g} \right) = 0. \tag{20}$$

Secondly, assume the function $Q = Q(q(x, t))$ to be either a flux or a density in the conservation law and define the average of function Q in the form of

$$\langle Q \rangle = \lim_{L \rightarrow \infty} \frac{1}{2L} \int_{-L}^L Q(q(x, t)) dx. \tag{21}$$

In order to describe the modulated waves, two scales should be introduced: a fast scale (x, t) and a slow scale $(X = \epsilon x, T = \epsilon t)$ with ϵ small. As done in FFM approach (Flaschka et al. 1980), the phase parameters κ_j and ω_j depend only on the slow variables (X, T) , but not on the fast variables (x, t) . Moreover, the Riemann invariants λ_i ($i = 1, 2, \dots, 2N + 2$) also depend only on the slow variables (X, T) . However, during the averaging procedure, the slow variables (X, T) are frozen. The integral (21) over the spatial variable x can be replaced by the integral over the N -torus as parameterized by the phases θ_j ($j = 1, 2, \dots, N$) variables provided the spatial wave numbers κ_j are incommensurate (see Eq. (19)). Thus the integral (21) is written as

$$\langle Q \rangle = \frac{1}{(2\pi)^m} \int_0^{2\pi} \cdots \int_0^{2\pi} Q(q(\theta_1, \theta_2, \dots, \theta_N)) d\theta_1 d\theta_2 \dots d\theta_N, \tag{22}$$

which is further transformed to the integration over the variables μ_j ($j = 1, 2, \dots, N$) in Dubrovin-type equation (17)

$$\langle Q \rangle = \frac{1}{(2\pi)^m} \int_{C_1} \cdots \int_{C_N} Q \frac{\partial(\theta)}{\partial(\mu)} d\mu_1 d\mu_2, \dots, d\mu_N, \tag{23}$$

where C_j ($j = 1, 2, \dots, N$) are the cycles defined by Abel maps and $\frac{\partial\theta}{\partial\mu}$ is the Jacobian (Flaschka et al. 1980) defined below

$$\frac{1}{(2\pi)^m} \frac{\partial(\theta)}{\partial(\mu)} = \frac{1}{V} \frac{\prod_{n>k}(\mu_n - \mu_k)}{\sqrt{\prod_{j=1}^N P(\mu_j)}}, \tag{24}$$

where V is a constant.

Thirdly, imposing the definition of the integral (21) on the conservation law (20) and considering the Riemann invariants λ_i ($i = 1, 2, \dots, 2N + 2$) as functions of the slow variables X and T give rise to

$$\left\langle \frac{G}{g} \right\rangle \frac{\partial \lambda_i}{\partial T} - \left\langle \frac{B}{g} \right\rangle \frac{\partial \lambda_i}{\partial X} = 0, \quad i = 1, 2, \dots, 2N + 2. \tag{25}$$

Finally, reminding the average defined in (23) and canceling the small quantity ϵ in Eq. (25) the desired Whitham equations for Riemann invariants λ_i ($i = 1, 2, \dots, 2N + 2$) are obtained as follows (Kamchatnov 1994)

$$\frac{\partial \lambda_i}{\partial t} + v_i(\lambda_1, \lambda_2, \dots, \lambda_{2N+2}) \frac{\partial \lambda_i}{\partial x} = 0, \quad i = 1, 2, \dots, 2N + 2, \tag{26}$$

where the characteristic velocities v_i are given by

$$\begin{aligned}
 v_i(\lambda_1, \lambda_2, \dots, \lambda_{2N+2}) &= -\frac{I_2(\lambda_1, \lambda_2, \dots, \lambda_{2N+2})}{I_1(\lambda_1, \lambda_2, \dots, \lambda_{2N+2})}, \\
 I_1(\lambda_1, \lambda_2, \dots, \lambda_{2N+2}) &= \int_{C_1} \cdots \int_{C_N} \frac{G}{g} \frac{\partial(\theta)}{\partial(\mu)} d\mu_1 d\mu_2 \cdots d\mu_N, \\
 I_2(\lambda_1, \lambda_2, \dots, \lambda_{2N+2}) &= \int_{C_1} \cdots \int_{C_N} \frac{B}{g} \frac{\partial(\theta)}{\partial(\mu)} d\mu_1 d\mu_2 \cdots d\mu_N. \tag{27}
 \end{aligned}$$

In the following three subsections, we will take $N = 0, N = 1$ and $N = 2$ to investigate the zero-phase, one-phase, and two-phase solutions of the defocusing cmKdV equation (1), respectively.

2.1 Zero-Phase Solution and Whitham Equations

For $N = 0$, take f to be degree one polynomial in spectral parameter λ and g, h to be functions independent of λ , i.e.,

$$f(x, t, \lambda) = \lambda + f_0(x, t), \quad g(x, t, \lambda) = g_0(x, t), \quad h(x, t, \lambda) = h_0(x, t). \tag{28}$$

Substituting them into Eqs. (8)–(9) and collecting the coefficients of λ yield

$$f_0(x, t) = \text{constant}, \quad g_0(x, t) = q(x, t), \quad h_0(x, t) = q^*(x, t), \tag{29}$$

and

$$\varepsilon q_x = 2iqf_0, \quad \varepsilon q_t = (12if_0\rho_0 + 8if_0^3)q, \tag{30}$$

with $\rho_0 = |q|^2$, which has exact solution of the form

$$q = \sqrt{\rho_0} e^{\frac{2if_0}{\varepsilon} [x + (6\rho_0 + 4f_0^2)t]}. \tag{31}$$

This is the zero-phase solution of the defocusing cmKdV equation (1), in which the function

$$\theta_0 = \frac{2f_0}{\varepsilon} \left[x + (6\rho_0 + 4f_0^2)t \right] \tag{32}$$

is a fast variable. The density ρ_0 and phase velocity $-(6\rho_0 + 4f_0^2)$ are slowly varying, and we have $\phi = 2f_0x$ and $v = 2f_0$ in the Madelung transformation (2).

In viewing the form of functions f, g and h , we have

$$f^2 - gh = \lambda^2 + 2f_0\lambda + f_0^2 - \rho = \lambda^2 - s_1\lambda + s_2, \tag{33}$$

where $s_1 = -2f_0$ and $s_2 = f_0^2 - \rho$. Moreover, assume the term $f^2 - gh$ has two roots λ_1 and λ_2 , i.e., $f^2 - gh = P(\lambda) = (\lambda - \lambda_1)(\lambda - \lambda_2)$, then we have

$$\lambda_1 + \lambda_2 = s_1, \quad \lambda_1\lambda_2 = s_2. \tag{34}$$

The equality $f_0 = v/2$ gives $s_1 = -v$ and $s_2 = v^2/4 - \rho$, so the equation (34) can be rewritten as

$$\lambda_1 + \lambda_2 = -v, \quad \lambda_1 \lambda_2 = v^2/4 - \rho, \tag{35}$$

which can be solved for λ_1 and λ_2 as

$$\lambda_1 = -\frac{v}{2} - \sqrt{\rho}, \quad \lambda_2 = -\frac{v}{2} + \sqrt{\rho}. \tag{36}$$

In order to derive the Whitham equation for the slow variables λ_1 and λ_2 , we transform the conservation law (13) into

$$\frac{\partial}{\partial t} \left(\sqrt{P(\lambda)} \frac{G}{g} \right) - \frac{\partial}{\partial x} \left(\sqrt{P(\lambda)} \frac{B}{g} \right) = 0. \tag{37}$$

In the sense of zero-phase solution (31), the modified conservation law (37) is simplified to

$$\frac{\partial}{\partial t} (\sqrt{P(\lambda)}) - \frac{\partial}{\partial x} (\sqrt{P(\lambda)} (4\lambda^2 - 2\lambda v + 2\rho + v^2)) = 0. \tag{38}$$

Expanding the partial derivatives in the above equation and taking limits $\lambda \rightarrow \lambda_1$ and $\lambda \rightarrow \lambda_2$, respectively, yield the Whitham equations for the slow variables λ_1 and λ_2 as follows:

$$\begin{aligned} \frac{\partial \lambda_1}{\partial t} - \left(\frac{15\lambda_1^2}{2} + 3\lambda_1 \lambda_2 + \frac{3\lambda_2^2}{2} \right) \frac{\partial \lambda_1}{\partial x} &= 0, \\ \frac{\partial \lambda_2}{\partial t} - \left(\frac{15\lambda_2^2}{2} + 3\lambda_1 \lambda_2 + \frac{3\lambda_1^2}{2} \right) \frac{\partial \lambda_2}{\partial x} &= 0. \end{aligned} \tag{39}$$

2.2 One-Phase Periodic Solution and Whitham Equations

It suffices to suppose that $P(\lambda)$ is a polynomial of degree four in λ for the one-phase periodic solution, that is

$$\begin{aligned} f^2 - gh &= P(\lambda) = \prod_{i=1}^4 (\lambda - \lambda_i) \\ &= \lambda^4 - s_1 \lambda^3 + s_2 \lambda^2 - s_3 \lambda + s_4, \end{aligned} \tag{40}$$

where s_i ($i = 1, 2, 3, 4$) are called elementary symmetric polynomials related to the four roots of the polynomial $P(\lambda)$. Recalling the Eqs. (8)–(9) for f , g and h , one has

$$f = \lambda^2 - f_1 \lambda + f_2, \quad g = q(\lambda - \mu), \quad h = q^*(\lambda - \mu^*), \tag{41}$$

where

$$\begin{aligned} f_{1x} &= f_{1t} = 0, \quad \varepsilon f_{2x} = i|q|^2(\mu - \mu^*), \\ \varepsilon f_{2t} &= 2i|q|^4(\mu - \mu^*) - i\varepsilon^2 q q_{xx}^* \mu + i\varepsilon^2 q^* q_{xx} \mu^*, \end{aligned} \tag{42}$$

and

$$\varepsilon q_x = 2iq(\mu - f_1), \quad \varepsilon^2 q_{xx} = -2i(2iqf_2 + q_x f_1 \varepsilon), \tag{43}$$

$$\varepsilon q_t = 2i\varepsilon^2 q_{xx} f_1 + 2\varepsilon(|q|^2 q_x - q_x^* q^2 - 2q_x f_2) + 4i|q|^2 q(\mu - f_1), \tag{44}$$

$$\varepsilon(q\mu)_x = -2iqf_2, \quad \varepsilon(q\mu)_t = 2i\varepsilon^2 q_{xx} f_2 + 2\varepsilon\mu(q_x |q|^2 - q_x^* q^2) - 4if_2 |q|^2 q, \tag{45}$$

as well as the complex conjugate of all coefficients of Eq. (41). Substituting Eq. (41) into Eq. (40) and comparing the coefficients of λ^k , the condition (41) gives the conservation laws

$$s_1 = 2f_1, \quad s_2 = -|q|^2 + f_1^2 + 2f_2, \quad s_3 = 2f_1 f_2 - |q|^2(\mu + \mu^*), \quad s_4 = f_2^2 - |q|^2 \mu \mu^*, \tag{46}$$

which indicates that $f_1 = s_1/2$, $f_2 = (|q|^2 - f_1^2 + s_2)/2$. Thus Eq. (42) for f_2 can be reduced to

$$\varepsilon \rho_x = 2i\rho(\mu - \mu^*), \quad \varepsilon \rho_t = 2i\rho(\mu - \mu^*)\left(\frac{3}{2}s_1^2 - 2s_2\right), \tag{47}$$

where $\rho = |q|^2$ and the evolution of μ can be expressed by Eq. (45) for μ as

$$\varepsilon \mu_x = -2if(\mu) = -2i\sqrt{P(\mu)}, \quad \varepsilon \mu_t = -2if(\mu)\left(\frac{3}{2}s_1^2 - 2s_2\right), \tag{48}$$

in which the second equality of the first equation (48) can be achieved by substituting $\lambda = \mu$ into Eq. (40). The relations given by Eqs. (47)–(48) indicate that μ and ρ depend on the phase

$$\xi = x - Vt, \quad \text{with } V = 2s_2 - \frac{3}{2}s_1^2. \tag{49}$$

Notice that the defocusing cmKdV equation (1) is the second flow in the defocusing NLS hierarchy, thus following the procedure of Appendix B.1 in the book of Kamchatnov (2000), the one-phase periodic solution $\rho = |q|^2$ can be expressed in term of the elliptic function

$$\rho = \rho_3 + (\rho_2 - \rho_3)\text{sn}^2\left(\frac{\sqrt{\rho_1 - \rho_3}}{\varepsilon}(\xi - \xi_0), m\right), \tag{50}$$

where sn is the Jacobi elliptic function, the modulus $m = (\rho_2 - \rho_3)/(\rho_1 - \rho_3)$, the parameter ξ_0 is the phase shift which is actually equal to zero in this work, and the

parameters ρ_1, ρ_2, ρ_3 are

$$\begin{aligned}\rho_1 &= \frac{1}{4}(\lambda_1 + \lambda_2 - \lambda_3 - \lambda_4)^2, \\ \rho_2 &= \frac{1}{4}(\lambda_1 - \lambda_2 + \lambda_3 - \lambda_4)^2, \\ \rho_3 &= \frac{1}{4}(\lambda_1 - \lambda_2 - \lambda_3 + \lambda_4)^2,\end{aligned}\quad (51)$$

from which it is easy to see that $\rho_1 > \rho_2 > \rho_3$ provided that $\lambda_1 > \lambda_2 > \lambda_3 > \lambda_4$.

Reminding the derivation of the Whitham equations in Eqs. (26) and (27), the Whitham equations corresponding to the one-phase periodic solution (50) are obtained as

$$\frac{\partial \lambda_i}{\partial t} - \frac{I_2(\lambda_1, \lambda_2, \lambda_3, \lambda_4)}{I_1(\lambda_1, \lambda_2, \lambda_3, \lambda_4)} \frac{\partial \lambda_i}{\partial x} = 0, \quad i = 1, 2, 3, 4, \quad (52)$$

where

$$I_1 = \frac{2}{\varepsilon} \frac{\partial L}{\partial \lambda_i}, \quad I_2 = \left(\frac{3}{2} s_1^2 - 2s_2 \right) I_1 + \frac{2}{\varepsilon} (s_1 + 2\lambda_i) L, \quad (53)$$

where the L represents the wavelength of the one-phase periodic solution (50), i.e.,

$$L = \frac{2\varepsilon K(m)}{\sqrt{(\lambda_1 - \lambda_3)(\lambda_2 - \lambda_4)}}, \quad (54)$$

where $K(m)$ is the complete elliptic integral of the first kind and the modulus m of the elliptic function is

$$m = \frac{\rho_2 - \rho_3}{\rho_1 - \rho_3} = \frac{(\lambda_1 - \lambda_2)(\lambda_3 - \lambda_4)}{(\lambda_1 - \lambda_3)(\lambda_2 - \lambda_4)}. \quad (55)$$

Finally, substituting the wavelength L formulated by Eq. (54) into Eqs. (52)–(53) the Whitham equations for the one-phase periodic solution (50) can be rewritten explicitly

$$\frac{\partial \lambda_i}{\partial t} + v_i(\lambda_1, \lambda_2, \lambda_3, \lambda_4) \frac{\partial \lambda_i}{\partial x} = 0, \quad i = 1, 2, 3, 4, \quad (56)$$

where the characteristic velocities $v_i = v_i(\lambda_1, \lambda_2, \lambda_3, \lambda_4)$ ($i = 1, 2, 3, 4$) are

$$\begin{aligned}
 v_1 &= - \left(\sum_{i < j} \lambda_i \lambda_j + \frac{3}{2} \sum_{i=1}^4 \lambda_i^2 \right) - \left(\sum_{i=1}^4 \lambda_i + 2\lambda_1 \right) \frac{2(\lambda_1 - \lambda_2)(\lambda_1 - \lambda_4)K(m)}{(\lambda_1 - \lambda_4)K(m) + (\lambda_4 - \lambda_2)E(m)}, \\
 v_2 &= - \left(\sum_{i < j} \lambda_i \lambda_j + \frac{3}{2} \sum_{i=1}^4 \lambda_i^2 \right) + \left(\sum_{i=1}^4 \lambda_i + 2\lambda_2 \right) \frac{2(\lambda_1 - \lambda_2)(\lambda_2 - \lambda_3)K(m)}{(\lambda_2 - \lambda_3)K(m) + (\lambda_3 - \lambda_1)E(m)}, \\
 v_3 &= - \left(\sum_{i < j} \lambda_i \lambda_j + \frac{3}{2} \sum_{i=1}^4 \lambda_i^2 \right) - \left(\sum_{i=1}^4 \lambda_i + 2\lambda_3 \right) \frac{2(\lambda_2 - \lambda_3)(\lambda_3 - \lambda_4)K(m)}{(\lambda_2 - \lambda_3)K(m) + (\lambda_4 - \lambda_2)E(m)}, \\
 v_4 &= - \left(\sum_{i < j} \lambda_i \lambda_j + \frac{3}{2} \sum_{i=1}^4 \lambda_i^2 \right) + \left(\sum_{i=1}^4 \lambda_i + 2\lambda_4 \right) \frac{2(\lambda_1 - \lambda_4)(\lambda_3 - \lambda_4)K(m)}{(\lambda_1 - \lambda_4)K(m) + (\lambda_3 - \lambda_1)E(m)},
 \end{aligned}
 \tag{57}$$

where $E(m)$ is complete elliptic integral of the second kind.

2.3 Two-Phase Periodic Solution and Whitham Equations

In this subsection, Kamchatnov’s way (Kamchatnov 1997) is carried out to explore the two-phase periodic solution and the corresponding Whitham equations for the defocusing cmKdV equation (1). In doing so, take $P(\lambda)$ to be a polynomial of degree six in λ

$$\begin{aligned}
 f^2 - gh &= P(\lambda) = \prod_{i=1}^6 (\lambda - \lambda_i) \\
 &= \lambda^6 - s_1 \lambda^5 + s_2 \lambda^4 - s_3 \lambda^3 + s_4 \lambda^2 - s_5 \lambda + s_6,
 \end{aligned}
 \tag{58}$$

where $\lambda_1 > \lambda_2 > \lambda_3 > \lambda_4 > \lambda_5 > \lambda_6$ are six roots and s_i ($i = 1, 2, \dots, 6$) are the elementary symmetric polynomials related to the six roots λ_i ($i = 1, 2, \dots, 6$), furthermore s_1 and s_2 are

$$s_1 = \sum_{j=1}^6 \lambda_j, \quad s_2 = \sum_{i,j=1; i \neq j}^6 \lambda_i \lambda_j.
 \tag{59}$$

Recalling the Eqs. (14)–(15) for f , g and h , we have

$$f = \lambda^3 - f_1 \lambda^2 + f_2 \lambda - f_3, \quad g = q(\lambda - \mu_1)(\lambda - \mu_2), \quad h = q^*(\lambda - \mu_1^*)(\lambda - \mu_2^*).
 \tag{60}$$

Thus Eq. (58) along with Eq. (60) further gives

$$s_1 = 2f_1, \quad s_2 = 2f_2 + f_1^2 - |q|^2.
 \tag{61}$$

In a similar way, the Dubrovin-type equation for functions $\mu_1(x, t)$ and $\mu_2(x, t)$ can be formulated from Eq. (17) for $N = 2$. Substituting the f, g and h in Eq. (60) into equation $\varepsilon g_x = 2iGf + 2Fg$ and collecting the coefficients of λ yields

$$\begin{aligned} \varepsilon q_x &= 2iq(\mu_1 + \mu_2 - f_1), \quad \varepsilon(q\mu_1)_x + \varepsilon(q\mu_2)_x = 2iq(\mu_1\mu_2 - f_2), \\ \varepsilon(q\mu_1\mu_2)_x &= -2iqf_3. \end{aligned}$$

The same substitution can be done for equation $\varepsilon g_t = 2iBf + 2Ag$ and one arrives at the “trace formula” for function $q(x, t)$ from Eq. (18) with $N = 2$, which finally gives rise to the two-phase periodic solution of the defocusing cmKdV equation (1) with phase functions

$$\theta_1 = \kappa_1 x + \omega_1 t + \theta_{01}, \quad \theta_2 = \kappa_2 x + \omega_2 t + \theta_{02}. \tag{62}$$

Next we return to the construction of the Whitham equations for this two-phase periodic solution. Recalling that $g = q(\lambda - \mu_1)(\lambda - \mu_2)$ one has

$$\begin{aligned} \frac{G}{g} &= \frac{1}{(\lambda - \mu_1)(\lambda - \mu_2)}, \\ \frac{B}{g} &= \frac{1}{(\lambda - \mu_1)(\lambda - \mu_2)} \\ &\quad \left[4\lambda^2 - 4\lambda \left(\mu_1 + \mu_2 - \frac{1}{2}s_1 \right) \right. \\ &\quad \left. - 4 \left(\frac{1}{2}\mu_1 s_1 + \frac{1}{2}\mu_2 s_1 - \mu_1 \mu_2 \right) + \frac{3}{2}s_1^2 - 2s_2 \right]. \end{aligned} \tag{63}$$

Therefore, following Kamchatnov’s way (Kamchatnov 1997) which is based on the general procedure of FFM approach (Flaschka et al. 1980), the Whitham equations for two-phase periodic solution can be derived as

$$\frac{\partial \lambda_i}{\partial t} + v_i(\lambda_1, \lambda_2, \lambda_3, \lambda_4, \lambda_5, \lambda_6) \frac{\partial \lambda_i}{\partial x} = 0, \quad i = 1, 2, \dots, 6, \tag{64}$$

where the characteristic velocities v_i ($i = 1, 2, \dots, 6$) are given by

$$v_i(\lambda_1, \lambda_2, \lambda_3, \lambda_4, \lambda_5, \lambda_6) = -\frac{I_2(\lambda_1, \lambda_2, \lambda_3, \lambda_4, \lambda_5, \lambda_6)}{I_1(\lambda_1, \lambda_2, \lambda_3, \lambda_4, \lambda_5, \lambda_6)}, \tag{65}$$

where $I_1 = I_1(\lambda_1, \lambda_2, \lambda_3, \lambda_4, \lambda_5, \lambda_6)$ and $I_2 = I_2(\lambda_1, \lambda_2, \lambda_3, \lambda_4, \lambda_5, \lambda_6)$ are

$$\begin{aligned} I_1 &= \int_{C_1} \frac{d\mu}{\sqrt{P(\mu)}} \int_{C_2} \frac{d\mu}{(\lambda_i - \mu)\sqrt{P(\mu)}} - \int_{C_2} \frac{d\mu}{\sqrt{P(\mu)}} \int_{C_1} \frac{d\mu}{(\lambda_i - \mu)\sqrt{P(\mu)}}, \\ I_2 &= \left(\frac{3}{2}s_1^2 - 2s_2 \right) I_1(\lambda_i) \\ &\quad + \int_{C_1} \int_{C_2} \frac{\left[4\lambda^2 - 4\lambda \left(\mu_1 + \mu_2 - \frac{1}{2}s_1 \right) - 4 \left(\frac{1}{2}\mu_1 s_1 + \frac{1}{2}\mu_2 s_1 - \mu_1 \mu_2 \right) + \frac{3}{2}s_1^2 - 2s_2 \right] (\mu_2 - \mu_1)}{(\lambda_i - \mu_1)(\lambda_i - \mu_2)\sqrt{P(\mu_1)P(\mu_2)}} d\mu_1 d\mu_2, \end{aligned}$$

where $P(\mu) = \prod_{i=1}^6(\mu - \lambda_i)$, and C_1 and C_2 are the cycles defining the solution of genus-2 Dubrovin-type equation (i.e., Eq. (18) with $N = 2$) according to the Abel transform. In our case, C_1 is cycle from λ_5 to λ_4 and C_2 is cycle from λ_3 to λ_2 . After tedious calculations, it is found that the characteristic velocities v_i ($i = 1, 2, \dots, 6$) are rewritten as

$$v_i(\lambda_1, \lambda_2, \lambda_3, \lambda_4, \lambda_5, \lambda_6) = 2s_2 - \frac{3}{2}s_1^2 - (4\lambda_i + 2s_1) \times \frac{[(\partial U_{11}/\partial \lambda_i)U_{21} - (\partial U_{21}/\partial \lambda_i)U_{11}] + 4(\partial U_{12}/\partial \lambda_i)(\partial U_{23}/\partial \lambda_i) - 4(\partial U_{13}/\partial \lambda_i)(\partial U_{22}/\partial \lambda_i)}{U_{11}(\partial U_{21}/\partial \lambda_i) - U_{21}(\partial U_{11}/\partial \lambda_i)}, \tag{66}$$

where U_{ij} are the hyperelliptic integrals

$$U_{ij} = \int_{C_i} \frac{\mu^{j-1}}{\sqrt{P(\mu)}} d\mu, \quad i = 1, 2; \quad j = 1, 2, 3.$$

3 Basic Wave Structures

This section starts to study what kinds of basic wave structures will appear for the defocusing cmKdV equation (1) with the general step-like initial data

$$q(x, 0) = \sqrt{\rho(x, 0)}e^{i\phi(x, 0)/\varepsilon}, \quad \phi_x(x, 0) = v(x, 0), \tag{67}$$

where $\rho(x, 0)$ and $v(x, 0)$ are

$$\rho(x, 0) = \begin{cases} \rho^r, & x > 0, \\ \rho^l, & x < 0, \end{cases} \quad \text{and} \quad v(x, 0) = \begin{cases} v^r, & x > 0, \\ v^l, & x < 0, \end{cases} \tag{68}$$

where ρ^r, ρ^l, v^r and v^l are four arbitrary real constants. The solution under the initial data (67) with (68) consisting of basic structures of rarefaction wave and dispersive shock wave are quite fruitful, which will be discussed in details below.

3.1 Rarefaction Waves

The genus-0 Whitham equation (39) corresponding to the zero-phase solution (31) can also be derived in a different way. To be specific, the rarefaction wave solution can be derived by taking the dispersionless limit as $\varepsilon \rightarrow 0$ for the dispersive hydrodynamics-like system (3) due to the property of smoothness itself. The system governing the rarefaction wave satisfies the following non-strictly hyperbolic system

$$\begin{cases} \rho_t - (3\rho^2 + 3v^2\rho)_x = 0, \\ v_t - (6\rho v + v^3)_x = 0. \end{cases} \tag{69}$$

This limit provides the solution correctly up to the solution develops to a shock. A standard procedure shows that the system (69) can be transformed into diagonal form

$$(r_{\pm})_t + V_{\pm}(r_+, r_-)(r_{\pm})_x = 0, \tag{70}$$

which is the genus-0 Whitham equation equivalent to the Whitham equation (39) under the scale transformation $r_+ = -\lambda_1, r_- = -\lambda_2$, where the Riemann invariants r_+ and r_- are

$$r_+ = \frac{v}{2} + \sqrt{\rho}, \quad r_- = \frac{v}{2} - \sqrt{\rho}, \tag{71}$$

and the characteristic velocities in terms of the Riemann invariants are expressed by

$$V_+ = -\left(\frac{15}{2}r_+^2 + 3r_+r_- + \frac{3}{2}r_-^2\right), \quad V_- = -\left(\frac{15}{2}r_-^2 + 3r_+r_- + \frac{3}{2}r_+^2\right). \tag{72}$$

Thus the initial data (67) with (68) in physical variables can be converted into the forms of Riemann invariants with the aid of the transformation (71)

$$r_+(x, 0) = \begin{cases} r_+^r = \frac{v^r}{2} + \sqrt{\rho^r}, & x > 0, \\ r_+^l = \frac{v^l}{2} + \sqrt{\rho^l}, & x < 0, \end{cases} \quad r_-(x, 0) = \begin{cases} r_-^r = \frac{v^r}{2} - \sqrt{\rho^r}, & x > 0, \\ r_-^l = \frac{v^l}{2} - \sqrt{\rho^l}, & x < 0. \end{cases} \tag{73}$$

Introducing the self-similar variable $\tau = x/t$, the Whitham equations (70) are rewritten as

$$(V_+ - \tau) \frac{dr_+}{d\tau} = 0, \quad (V_- - \tau) \frac{dr_-}{d\tau} = 0. \tag{74}$$

Similar to the case of the defocusing NLS equation (El et al. 1995), the bi-directionality determines three cases of rarefaction waves, i.e., only r_+ is a constant, only r_- is a constant, and both r_+ and r_- are constants. However, different from the defocusing NLS case, the characteristic of the defocusing cmKdV equation (1) propagates along single direction and divides into five types basic rarefaction wave structures. The first two types are

$$r_+ = r_+^0 = \text{constant}, \quad r_- = -\frac{1}{5}r_+^0 \pm \frac{1}{15}\sqrt{-36(r_+^0)^2 - 30 \cdot \frac{x}{t}}, \tag{75}$$

and the characteristic velocity $V_- = V_-(r_+^0, r_-)$. The middle two types are

$$r_+ = -\frac{1}{5}r_-^0 \pm \frac{1}{15}\sqrt{-36(r_-^0)^2 - 30 \cdot \frac{x}{t}}, \quad r_- = r_-^0 = \text{constant}, \tag{76}$$

with the velocity $V_+ = V_+(r_+, r_-^0)$, and the fifth type is

$$r_+ = \frac{1}{\sqrt{6}}\sqrt{-\frac{x}{t}}, \quad r_- = -\frac{1}{\sqrt{6}}\sqrt{-\frac{x}{t}}, \tag{77}$$

with the velocities $V_+ = V_+(r_+, r_-) = \tau = V_-$. It is observed that the evolution of Riemann invariants for any choice of the rarefaction waves will be on the parabola

$$\frac{15}{2}r^2 + 3rr^0 + \frac{3}{2}(r^0)^2 + \tau = 0 \tag{78}$$

for the cases in (75)–(76) and on the parabola

$$6r^2 + \tau = 0 \tag{79}$$

for the case in (77), which are displayed in blue dot lines in Fig. 1a–f. It is remarked that we denote r to represent the Riemann invariants r_{\pm} and λ_i ($i = 1, 2, \dots, 2N$) in all the figures in this work. As we shall see, there exists the case when two Riemann invariants collide, and the coalescence of the Riemann invariants results from the property of the defocusing cmKdV equation (1), i.e., not genuinely nonlinear [see Kodama et al. (2008)], which does not appear in the defocusing NLS case. In addition, we call the solution to be a plateau if both $r_+ =$ and $r_- =$ are constants. The pure rarefaction wave or the plateau, excluding any type of dispersive shock wave, will occur in three situations, i.e., $r_+^r \geq r_+^l \geq r_-^l \geq r_-^r \geq r^*$, $r_+^l \geq r_+^r \geq r^* \geq r_-^r \geq r_-^l$ and $r^* \geq r_+^r \geq r_+^l \geq r_-^r \geq r_-^l$, where r^* represents the point on which $\frac{\partial V_{\pm}}{\partial r}$ changes sign. Otherwise, the oscillating region will appear that will be discussed in the next subsection. The distributions of Riemann invariants along with the basic structures of rarefaction waves are shown in Fig. 1, which are denoted as {RW-I}, {RW-II}, ..., {RW-VI}, where “RW” is the abbreviation of rarefaction wave. The formation of the two parabolas in the third type of rarefaction wave degenerates to linearity eventually. It is remarked that the rarefaction wave structure {RW-III} is a new basic wave structure in the defocusing cmKdV equation (1), which has not been proposed by Kodama et al. (2008) and Kong et al. (2019) and other studies before.

Examples of the combination of rarefaction wave are demonstrated in Fig. 2, where the combined rarefaction wave consists of five regions, from left to right, which are plateau, {RW-II}, {RW-III}, {RW-I} and plateau again. The boundary velocity between each regions are given by analyzing the three cases of the rarefaction waves. In this example, they are separated by, from left to right, $x/t = -13.875, -6, -1.5, -0.3$, respectively. The combined rarefaction wave evolving from the initial condition $r_+^l = 1.5, r_+^r = 0.5, r_-^l = -1, r_-^r = -0.1$ displays excellent agreement with the direct numerical simulations; see Fig. 2b.

3.2 Dispersive Shock Waves

From the analysis of the last subsection, it is clear that the rarefaction wave solutions are valid for the defocusing cmKdV equation (1) until the wave breaking appears. The solution of equation (1) is governed by smooth enough rarefaction wave in term of two Riemann invariants, but soon after the breaking, one of the Riemann invariants develops into three branches governed by the averaging Whitham equation (56) and (57). The corresponding multi-valued region is replaced by an oscillating region. However, in the case of self-similar solution, the oscillating region can be determined

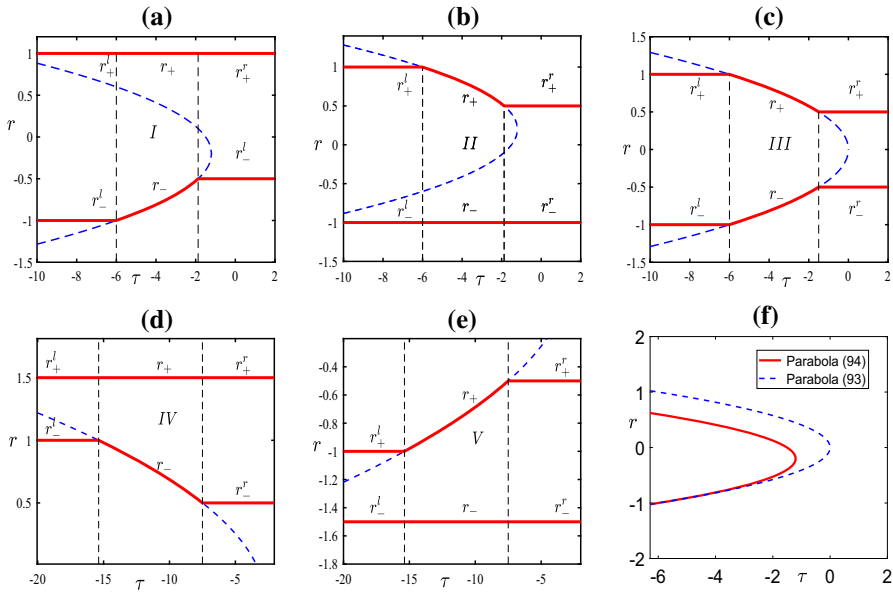


Fig. 1 (Color online) Sketches of Riemann invariants and five possible basic rarefaction waves structures: **a** $r_+^l = r_+^r = 1, r_-^l = -1, r_-^r = -0.5$; **b** $r_+^l = 1, r_+^r = 0.5, r_-^l = r_-^r = -1$; **c** $r_+^l = 1, r_+^r = 0.5, r_-^l = -1, r_-^r = -0.5$; **d** $r_+^l = r_+^r = 1.5, r_-^l = 1, r_-^r = 0.5$; **e** $r_+^l = -1, r_+^r = -0.5, r_-^l = r_-^r = -1.5$

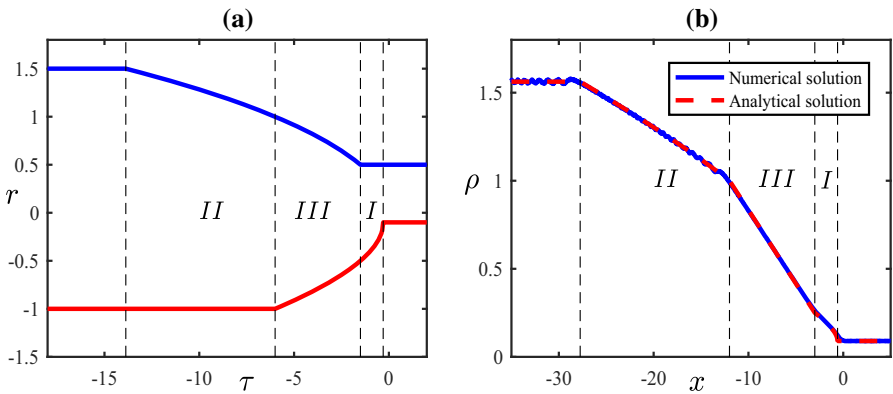


Fig. 2 (Color online) Examples of self-similar solution of the combined rarefaction wave at time $t = 2$. The initial condition is $r_+^l = 1.5, r_+^r = 0.5, r_-^l = -1, r_-^r = -0.1$: **a** distributions of the Riemann invariants; **b** comparison of the analytical solution from Whitham modulation theory with direct numerical simulations, where the red dashed line indicates analytical solution and the blue solid line represents the numerical solution

immediately once the initial data are given. In this subsection, all kinds of structures of basic DSWs that may appear in the defocusing cmKdV equation (1) will be discussed in details.

Let us now list the basic structures of DSWs possibly appearing in the defocusing cmKdV equation (1), in which part of them have been given in Kodama et al. (2008). The first four types of DSWs are similar to the defocusing NLS case, where three Riemann invariants are constants while the fourth one changes, either λ_2 or λ_3 . The reason for existing four types of DSWs in equation (1) instead of only two of them in the defocusing NLS case lies in the fact that there still exists a parametric parabola determined by three constants. Thus the four basic structures of DSWs can be obtained by truncating the upper or lower part of the parabola on each Riemann invariant λ_2 and λ_3 . The distributions of such kinds of Riemann invariants describing DSWs are displayed in Fig. 3. The second four types of DSW rising from the non-genuine nonlinear system (56) with (57) satisfy the solution in which two Riemann invariants are constants and the other two change, as shown in Fig. 4. For simplicity, denote the eight basic structures of DSWs as {DSW-I}, {DSW-II}, ..., {DSW-VIII}, respectively. The two black dotted lines in Figs. 3 and 4 represent two distinct speeds characterized the DSWs which is known as the leading and trailing speed of their edges. The leading and trailing speeds of two edges can be found from Eq. (57) by taking the limitation $m \rightarrow 1$ for $\lambda_3 = \lambda_2$, and $m \rightarrow 0$ for $\lambda_3 = \lambda_4$ or $\lambda_2 = \lambda_1$, respectively. In the eight basic structures of DSWs listed in Figs. 3 and 4, the spatial structure is divided into three regions, i.e., the plateau for $\frac{x}{t} < v|_{\text{left}}$, the DSW for $v|_{\text{left}} < \frac{x}{t} < v|_{\text{right}}$ and the plateau again for $\frac{x}{t} > v|_{\text{right}}$. It is remarked that the distributions of DSWs shown in Figs. 3 and 4 are obtained numerically via the scheme of two-step variant of Lax-Wendroff with nonlinear filter for the step-like function (Engquist et al. 1989).

For simplicity, we only analyze the boundary speeds of two types of DSWs, the other types can be explained easily in a similar way. For the case of {DSW-I}, it is seen that

$$\tau = \frac{x}{t} = v_3 \left(r_+^r, r_-^l, \lambda_3, r_-^r \right), \tag{80}$$

which indicates that the speeds of the right edge $\tau|_{\text{right}}$ and the left edge $\tau|_{\text{left}}$ can be expressed as

$$\tau|_{\text{right}} = v_3(r_+^r, r_-^l, \lambda_3, r_-^r)|_{\lambda_3=r_-^l}, \quad \tau|_{\text{left}} = v_3(r_+^r, r_-^l, \lambda_3, r_-^r)|_{\lambda_3=r_-^r}.$$

For the case of {DSW-V}, one has

$$\begin{aligned} \tau = \frac{x}{t} &= v_2(r_+^l, \lambda_2, \lambda_3, r_-^r), \quad \tau = \frac{x}{t} = v_3(r_+^l, \lambda_2, \lambda_3, r_-^r), \\ \tau|_{\text{left}} &= v_3(r_+^l, \lambda_2, \lambda_3, r_-^r)|_{\lambda_3=r_-^r}, \quad \tau|_{\text{right}} = v_2(r_+^l, \lambda_2, \lambda_3, r_-^r)|_{\lambda_3=\lambda_2}. \end{aligned} \tag{81}$$

It is noted that all of above cases are obviously the extension of the basic structures of rarefaction waves. The vertex of parabola r^* , at which the signs of $\partial v_i / \partial r$ ($i = 1, 2, 3, 4$) change, plays an important role in distinguishing the types of {DSW-I}-{DSW-IV} and the types of {DSW-V}-{DSW-VIII}. The regions of DSW in Fig. 4 include vertex of parabola r^* connecting the two Riemann invariants such as λ_2 and

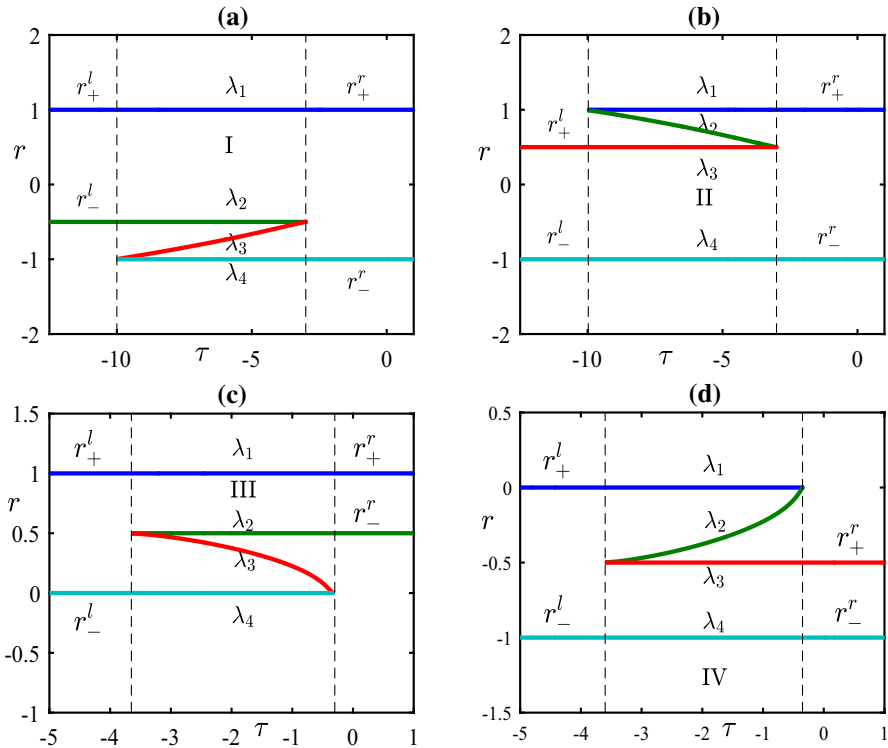


Fig. 3 (Color online) Four typical distributions of the Riemann invariants $\lambda_1, \lambda_2, \lambda_3,$ and λ_4 for the DSWs with only λ_2 or λ_3 varying. **a** Type I: $r_+^l = r_+^r = 1, r_-^l = -0.5, r_-^r = -1$; **b** Type II: $r_+^l = 0.5, r_+^r = 1, r_-^l = r_-^r = -1$; **c** Type III: $r_+^l = r_+^r = 1, r_-^l = 0, r_-^r = 0.5$; **d** Type IV: $r_+^l = 0, r_+^r = -0.5, r_-^l = r_-^r = -1$

λ_3 in Fig. 4a, b, λ_3 and λ_4 in Fig. 4c, λ_1 and λ_2 in Fig. 4d, and the vertex r^* in Fig. 4a, b can be determined by

$$\frac{\partial v_3(\lambda_1, r^*, r^*, \lambda_4)}{\partial r^*} = 0, \tag{82}$$

from which we arrive at $r^*(\lambda_1, \lambda_4) = -\frac{1}{4}(\lambda_1 + \lambda_4)$. The same way can be utilized to formulate the vertex r^* in Fig. 4c, d, which do not display here because of their complexity.

The remaining two basic structures of DSWs, i.e., {DSW-IX} and {DSW-X}, are the one people have never seen before including the pioneering work on the defocusing cmKdV equation (1) in Kodama et al. (2008) and have not been appear neither in the strictly hyperbolic system such as the defocusing NLS equation nor in the non-strictly hyperbolic system for which r_+ or r_- is constant. This kind of structure also requires two variables slowly varying, but importantly they must be on both sides of the parabola. Otherwise, it develops a combination of DSWs and rarefaction waves. For this case, we suffice to show that the velocity of leading edge in Fig. 5a (two

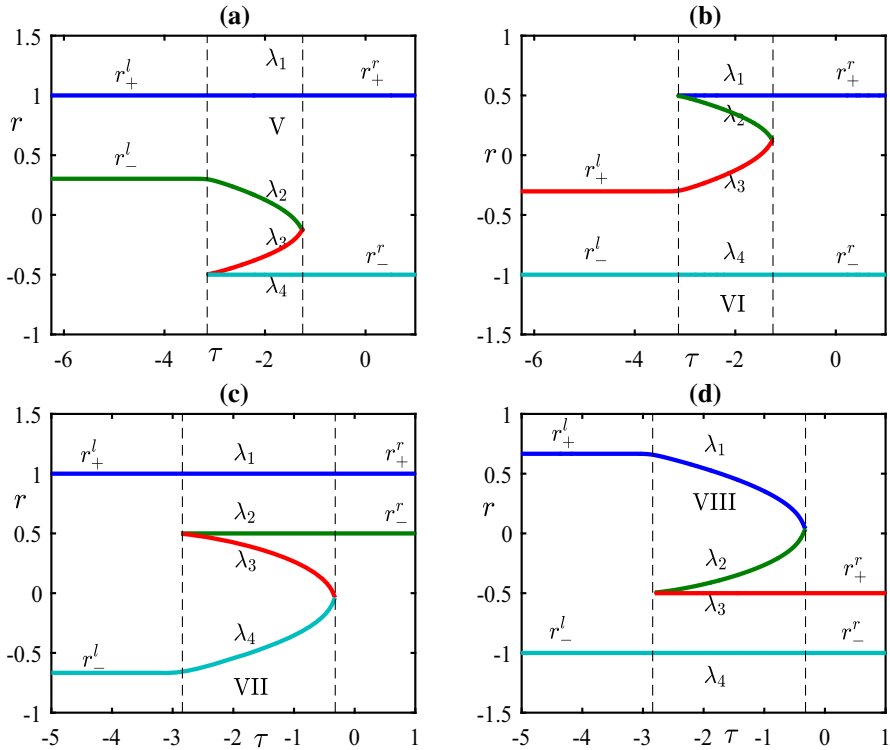


Fig. 4 (Color online) Four typical distributions of the Riemann invariants $\lambda_1, \lambda_2, \lambda_3,$ and λ_4 for the DSWs with two of them varying. **a** Type V: $r^* = -\frac{1}{8}, r_+^l = r_+^r = 1, r_-^l = -\frac{3}{2} + \frac{1}{2}\sqrt{13}, r_-^r = -0.5$; **b** Type VI: $r^* = \frac{1}{8}, r_+^l = \frac{3}{2} - \frac{1}{2}\sqrt{13}, r_+^r = 0.5, r_-^l = r_-^r = -1$; **c** Type VII: $r^* = -0.0378, r_+^l = r_+^r = 1, r_-^l = -\frac{2}{3}, r_-^r = 0.5$; **d** Type VIII: $r^* = 0.0378, r_+^l = \frac{2}{3}, r_+^r = -0.5, r_-^l = r_-^r = -1$

variable on the one side) is

$$v_3|_{\lambda_3=\lambda_2} = - \left(\frac{3}{2}\lambda_1^2 + 4\lambda_2^2 + \frac{3}{2}\lambda_4^2 + 2\lambda_1\lambda_2 + 2\lambda_2\lambda_4 + \lambda_1\lambda_4 \right). \tag{83}$$

One may find at once that it exactly coincide with the trailing speed of rarefaction wave when taking $\lambda_2 = \lambda_1$, thus we have

$$v_3|_{\lambda_3=\lambda_2, \lambda_2=\lambda_1} = - \left(\frac{15}{2}\lambda_1^2 + 3\lambda_1\lambda_4 + \frac{3}{2}\lambda_4^2 \right) = v_1|_{\lambda_3=\lambda_2}. \tag{84}$$

As followed from the last subsection, the velocity in (84) for the negative direction of the Riemann invariant λ_1 is an increasing function on the interval $[-\lambda_4/5, +\infty)$, i.e., the upper part of the parabola. The same procedure can be applied to Fig. 5b immediately.

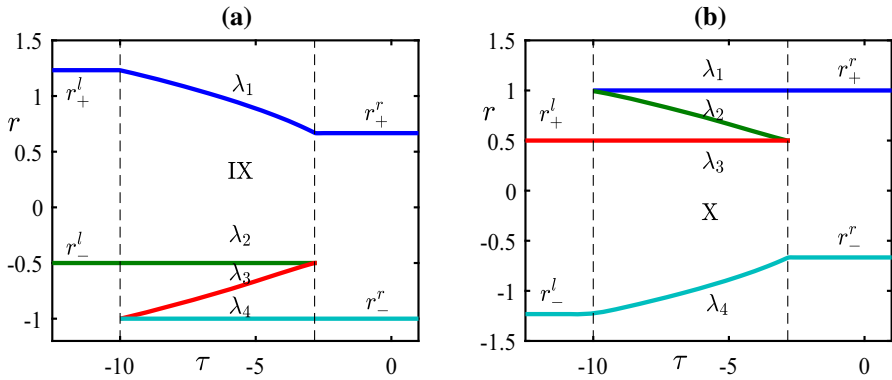


Fig. 5 (Color online) Two typical distributions of the Riemann invariants $\lambda_1, \lambda_2, \lambda_3,$ and λ_4 for the DSWs with two of them varying. **a** Type IX: $r_+^l = \sqrt{3} - \frac{1}{2}, r_+^r = \frac{2}{3}, r_-^l = -\frac{1}{2}, r_-^r = -1$; **b** Type X: $r_+^l = \frac{1}{2}, r_+^r = 1, r_-^l = \frac{1}{2} - \sqrt{3}, r_-^r = -\frac{2}{3}$

4 Complete Classification of the Solution to Riemann Problem

In the last section, five types of rarefaction waves and ten types of DSWs have been figured out, in which except for {RW-III} all basic wave structures have common feature with one of the initial data, i.e., either $r_+^l = r_+^r$ or $r_-^l = r_-^r$. With the fifteen basic wave structures at hand, we are ready to carry out the classification of the solutions for the defocusing cmKdV equation (1) with step-like initial data (67) with (68). In doing so, recall that $r_+ = \frac{v}{2} + \sqrt{\rho}$ and $r_- = \frac{v}{2} - \sqrt{\rho}$. Fixing the initial value (68) at the left-hand side (v^l, ρ^l), the Riemann invariants r_-^l and r_+^l are determined. So we have two parabolas

$$\rho = \left(r_+^l - \frac{v}{2}\right)^2 \quad \text{and} \quad \rho = \left(r_-^l - \frac{v}{2}\right)^2, \tag{85}$$

with vertexes $2r_+^l > 2r_-^l$ on the horizontal v -axis, which are shown in the solid lines in Fig. 6. It is observed that the two parabolas divide the (v, ρ) plane into six regions. The order among $r_+^l, r_-^l, r_+^r, r_-^r$ can be determined easily in each region. Taking the region F as an example, for a point $(v_F, \rho_F) = (v^r, \rho^r)$ in this region, similarly, two parabolas $\rho = (r_+^r - \frac{v}{2})^2$ and $\rho = (r_-^r - \frac{v}{2})^2$ with vertexes $2r_+^r > 2r_-^r$ are obtained, which are displayed in the dotted lines in Fig. 6. It is clear that $r_+^r > r_-^r > r_+^l > r_-^l$ in region F . The orders of the left and right Riemann invariants for the other regions can be found in the same way:

$$\begin{aligned} \mathbf{A.} & r_+^l > r_+^r > r_-^r > r_-^l, & \mathbf{B.} & r_+^l > r_+^r > r_-^l > r_-^r, \\ \mathbf{C.} & r_+^l > r_-^l > r_+^r > r_-^r, & \mathbf{D.} & r_+^r > r_+^l > r_-^l > r_-^r, \\ \mathbf{E.} & r_+^r > r_+^l > r_-^r > r_-^l, & \mathbf{F.} & r_+^r > r_-^r > r_+^l > r_-^l. \end{aligned} \tag{86}$$

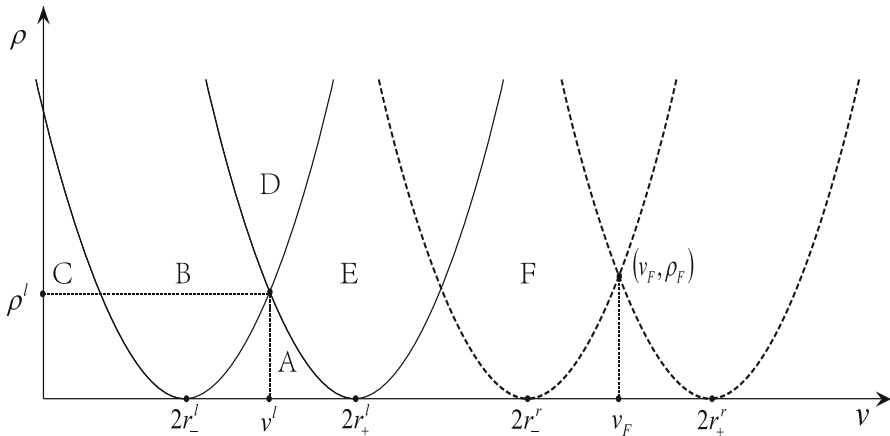


Fig. 6 Regions in the (v, ρ) plane corresponding to different classes of the solution for Riemann problem (67) with (68)

In this section, the complete classification of the solution for the Riemann problem of the defocusing cmKdV equation (1) are given by analyzing the six possible cases above based on the Whitham equations proposed in Sect. 2 and the basic wave structures in Sect. 3.

4.1 Case A. $r_+^l > r_+^r > r_-^r > r_-^l$

In each case, the vertexes of the parabolas (78) and (79) play a vital role in the classification of the solution for the Riemann problem of equation (1). In what follows, four subcases are discussed, which combine the complete classification of Case A.

4.1.1 Subcase A₁: $r_-^r > r^*$

Here the vertex of the parabola r^* satisfies

$$\frac{\partial v_3(r_+^l, r_-^r, r^*, r^*)}{\partial r^*} = 0. \tag{87}$$

Note that putting $r_-^r = r^*$ into (87) yields $r^* = -r_+^r/5$, which is the critical condition followed from Sect. 3.1, and the $r_+^l > r_+^r$ located in the upper part of parabola will develop to a rarefaction wave. The whole scenarios under this condition are analyzed in eight more cases, which are $A_{1,1} - A_{1,8}$. See Figs. 7, 8 and Table 1 for details.

- $A_{1,1}$: $r_+^l > r_+^r > r_-^r > r_-^l, r_-^l \geq r^*$.

In this case, the solution of the Riemann invariants consists of five regions (see Fig. 7a), and in each region, the Riemann invariants can be formulated below.

- (1) For $x/t \leq v_1(r_+^l, r_-^r, r_-^r, r_-^l)$, the solution is in the plateau region with Riemann invariants

$$r_+ = r_+^l, \quad r_- = r_-^l.$$

- (2) For $v_1(r_+^l, r_-^r, r_-^r, r_-^l) < x/t < v_1(r_+^r, r_-^r, r_-^r, r_-^l)$, the solution is in the {RW-II} region with Riemann invariants

$$r_+ = -\frac{1}{5}r_-^l + \frac{1}{15}\sqrt{-36(r_-^l)^2 - 30 \cdot \frac{x}{t}}, \quad r_- = r_-^l.$$

- (3) For $v_1(r_+^r, r_-^r, r_-^r, r_-^l) \leq x/t \leq v_3(r_+^r, r_-^r, r_-^r, r_-^l)$, the solution is in the plateau region with Riemann invariants

$$r_+ = r_+^r, \quad r_- = r_-^l.$$

- (4) For $v_3(r_+^r, r_-^r, r_-^r, r_-^l) < x/t < v_3(r_+^r, r_-^r, r_-^r, r_-^l)$, the solution is in the {DSW-III} region with Riemann invariants

$$\lambda_1 = r_+^r, \quad \lambda_2 = r_-^r, \quad \frac{x}{t} = v_3(r_+^r, r_-^r, \lambda_3, r_-^l), \quad \lambda_4 = r_-^l.$$

- (5) For $x/t \geq v_3(r_+^r, r_-^r, r_-^r, r_-^l)$, the solution is also in the plateau region with Riemann invariants

$$r_+ = r_+^r, \quad r_- = r_-^l.$$

Figure 7b shows that the analytical result from Whitham modulation theory agrees well with the direct numerical simulations.

- $A_{1,2} : r_+^l > r_+^r > r_-^r > r_-^l, \quad r_-^r > r^*, \quad r^* \geq r_-^l \geq r^{**}.$

Here the point r^{**} is determined by

$$v_3(r_+^r, r_-^r, r_-^r, r^{**}) = v_4(r_+^r, r_-^r, r_-^r, r^{**}). \tag{88}$$

The solution regions in this case is very similar to the case $A_{1,1}$, but the {DSW-III} region in case $A_{1,1}$ is divided into two combined DSWs, i.e., {DSW-III} and {DSW-VII}. The Riemann invariants corresponding to the regions of the two combined DSWs are formulated as follows.

For $v_3(r_+^r, r_-^r, r_-^r, r_-^l) < x/t < v_4(r_+^r, r_-^r, r_e^*, r_-^l)$, where r_e^* solves the implicit equation $v_3(r_+^r, r_-^r, r_e^*, r_-^l) = v_4(r_+^r, r_-^r, r_e^*, r_-^l)$, the solution is in the {DSW-III} region with Riemann invariants

$$\lambda_1 = r_+^r, \quad \lambda_2 = r_-^r, \quad \frac{x}{t} = v_3(r_+^r, r_-^r, \lambda_3, r_-^l), \quad \lambda_4 = r_-^l.$$

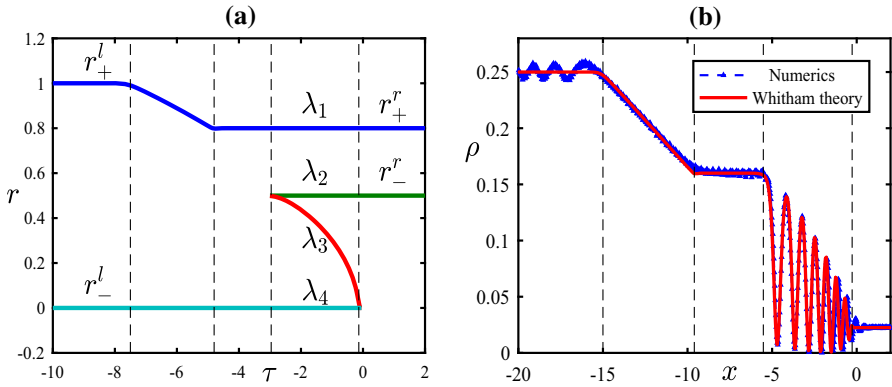


Fig. 7 (Color online) Example of the self-similar solution for case $A_{1.1}$ combined by {RW-II} and {DSW-III} with initial condition $r_+^l = 1, r_+^r = 0.8, r_-^l = 0, r_-^r = 0.5$ at time $t = 2$: **a** distributions of the Riemann invariants in five regions; **b** comparison of the analytical solution from Whitham modulation theory (solid red line) with direct numerical simulations (dash blue line)

For $v_4(r_+^r, r_-^r, r_e^*, r_-^l) \leq x/t \leq v_4(r_+^r, r_-^r, r^*, r^*)$, the solution is in the {DSW-VII} region with Riemann invariants

$$\lambda_1 = r_+^r, \quad \lambda_2 = r_-^r, \quad \frac{x}{t} = v_3(r_+^r, r_-^r, \lambda_3, \lambda_4), \quad \frac{x}{t} = v_4(r_+^r, r_-^r, \lambda_3, \lambda_4).$$

- $A_{1.3} : r_+^l > r_+^r > r_-^r > r_-^l, r_-^r > r^*, -r_+^r \leq r_-^l \leq r^{**}$.

This case emerges by dividing the intermediate plateau in case $A_{1.2}$ into a plateau and a {RW-I} rarefaction wave, where the other regions are similar to case $A_{1.2}$ except the {RW-I} region, whose Riemann invariants are expressed by

$$r_+ = r_+^r, \quad r_- = -\frac{1}{5}r_+^r - \frac{1}{15}\sqrt{-36(r_+^r)^2 - 30 \cdot \frac{x}{t}},$$

for $v_1(r_+^r, r_-^r, r_-^l, r_-^l) < x/t < v_4(r_+^r, r_-^r, r_-^r, r^{**})$.

- $A_{1.4} : r_+^l > r_+^r > r_-^r > r_-^l, r_-^r > r^*, -r_+^l \leq r_-^l \leq -r_+^r$.

This case comes from case $A_{1.3}$ by dividing the {RW-II} region into two different regions of rarefaction waves, i.e., {RW-II} and {RW-III}. The solution of Riemann invariants for {RW-II} region is the same as case $A_{1.3}$ for $v_1(r_+^l, r_-^r, r_-^r, r_-^l) < x/t < v_4(-r_-^l, r_-^r, r_-^r, r_-^l)$, but for $v_4(-r_-^l, r_-^r, r_-^r, r_-^l) < x/t < v_4(r_+^r, r_-^r, r_-^r, r_-^l)$, the solution is in the {RW-III} region with Riemann invariants

$$r_+ = \frac{1}{\sqrt{6}}\sqrt{-\frac{x}{t}}, \quad r_- = -\frac{1}{\sqrt{6}}\sqrt{-\frac{x}{t}}.$$

- $A_{1.5} : r_+^l > r_+^r > r_-^r > r_-^l, r_-^r > r^*, r_-^l < -r_+^l$.

This case emerges by dividing the left plateau in case $A_{1.4}$ into a plateau

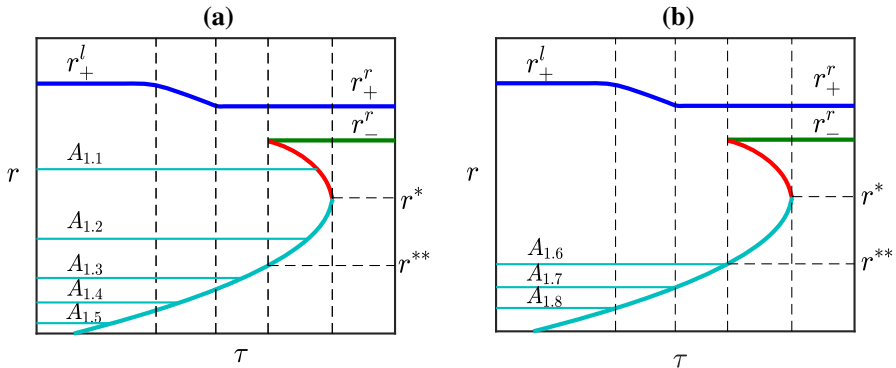


Fig. 8 (Color online) Distributions of Riemann invariants for all the possible cases in Case A_1 under the condition $r_-^r > r^*$: **a** the characteristic velocity r_+^l is chosen to divide the corresponding region into two smaller regions; **b** the characteristic velocity r_-^l is chosen to equal to the boundary velocities

Table 1 Classification of solutions and region distributions in eight subcases under condition A_1 , where “Null” means there does not exist this region

Cases	Regions					
	Region 1	Region 2	Region 3	Region 4	Region 5	Region 6
$A_{1,1}$	Plateau	{RW-II}	Plateau	{DSW-III}	Plateau	Null
$A_{1,2}$	Plateau	{RW-II}	Plateau	{DSW-III}	{DSW-VII}	Plateau
$A_{1,3}$	Plateau	{RW-II}	Plateau	{RW-I}	{DSW-VII}	Plateau
$A_{1,4}$	Plateau	{RW-II}	{RW-III}	{RW-I}	{DSW-VII}	Plateau
$A_{1,5}$	Plateau	{RW-I}	{RW-III}	{RW-I}	{DSW-VII}	Plateau
$A_{1,6}$	Plateau	{RW-II}	Plateau	{DSW-VII}	Plateau	Null
$A_{1,7}$	Plateau	{RW-II}	{RW-I}	{DSW-VII}	Plateau	Null
$A_{1,8}$	Plateau	{RW-III}	{RW-I}	{DSW-VII}	Plateau	Null

and a {RW-I} rarefaction wave, in which for $v_4(r_+^l, r_-^r, r_-^r, r_-^l) < x/t < v_1(r_+^l, r_-^r, r_-^r, -r_+^l)$, the solution is in the {RW-I} region with Riemann invariants

$$r_+ = r_+^l, \quad r_- = -\frac{1}{5}r_+^l - \frac{1}{15}\sqrt{-36(r_+^l)^2 - 30 \cdot \frac{x}{t}}$$

for $v_4(r_+^l, r_-^r, r_-^r, r_-^l) < x/t < v_1(r_+^l, r_-^r, r_-^r, -r_+^l)$.

The cases $A_{1,6} - A_{1,8}$, where the characteristic velocity r_-^l is chosen to equal to the boundary velocities, can also be analyzed in the same way. All these cases can be seen clearly in Fig. 8 and Table 1. It is remarked that all the descriptions of regions here and below are from left to right. For instance, the solution regions of case $A_{1,2}$ in Table 1 from left to right are Region 1 (plateau) to Region 6 (plateau).

4.1.2 Subcase A_2 : $r_+^r < r_{A_2}^*$

Here the critical point $r_{A_2}^*$ satisfies

$$\frac{\partial v_2(r_{A_2}^*, r_{A_2}^*, r_+^r, r_-^r)}{\partial r_{A_2}^*} = 0. \tag{89}$$

Substituting $r_+^r = r_{A_2}^*$ into equation (89) yields $r_{A_2}^* = -1/r_-^r$. The distributions of the Riemann invariants under condition A_2 are much similar to that under condition A_1 , moreover, the density ρ in each case of A_2 are exactly the same with that in case A_1 . Thus, we ignore the analysis and only list the results of the classification in this case. See Table 2 for details, where the other critical point $r_{A_2}^{**}$ solves the following implicit equation

$$v_1(r_{A_2}^{**}, r_+^r, r_+^r, r_-^r) = v_2(r_{A_2}^{**}, r_+^r, r_+^r, r_-^r). \tag{90}$$

In fact, the Riemann invariants in all the cases of A_1 and A_2 are symmetric with respect to x -axis. More specifically, {RW-II} in A_1 is symmetrical to {RW-I} in A_2 , {DSW-III} in A_1 is symmetrical to {DSW-IV} in A_2 , and {DSW-VII} in A_1 is symmetrical to {DSW-VIII} in A_2 , which can also be understood through equation (57) and the equality below:

$$\begin{aligned} v_1(\lambda_1^0, \lambda_2^0, \lambda_3^0, \lambda_4^0) &= v_4(-\lambda_4^0, -\lambda_3^0, -\lambda_2^0, -\lambda_1^0), \\ v_2(\lambda_1^0, \lambda_2^0, \lambda_3^0, \lambda_4^0) &= v_3(-\lambda_4^0, -\lambda_3^0, -\lambda_2^0, -\lambda_1^0). \end{aligned}$$

where λ_i^0 ($i = 1, 2, 3, 4$) represent constants (see equation (96) for details).

It is seen that DSWs emerge in both case A_1 and A_2 . In what follows, the case in which only plateau and rarefaction wave regions are produced is discussed under special conditions.

4.1.3 Subcase A_3 : $r_-^r \leq r^*$ and $r_+^r \geq r_{A_2}^*$

In this case, the solution regions only evolve the combination of plateau and rarefaction waves, which makes the classification to be simpler than cases A_1 and A_2 above. Firstly, all the possible cases under condition A_3 are listed in Table 3.

The classification of solutions and region distributions for the subcases listed in Table 3 are given in Table 4. It is remarked that except case $A_{3,42}$, which is in fact one of the basic rarefaction wave structures of {RW-III}, all cases evolve at least four regions. In each case, the boundary velocities can also be derived in the similar way. For simplicity, we only analyze $A_{3,31}$ in details, which are found in Sect. 3.1 and Fig. 2.

- (1) For $x/t < v_+(r_+^l, r_-^l)$, the solution is in the plateau region with Riemann invariants

$$r_+ = r_+^l, \quad r_- = r_-^l.$$

Table 2 Classification of solutions and region distributions in eight subcases under condition A_2

Conditions	Regions					
	Region 1	Region 2	Region 3	Region 4	Region 5	Region 6
$r_+^I \leq r_{A2}^{**}$	Plateau	{RW-I}	Plateau	{DSW-IV}	Plateau	Null
$r_{A2}^* < r_+^I < r_{A2}^{**}$	Plateau	{RW-I}	Plateau	{DSW-IV}	{DSW-VIII}	Plateau
$r_{A2}^{**} < r_+^I < -r_-^I$	Plateau	{RW-I}	Plateau	{RW-II}	{DSW-VIII}	Plateau
$-r_-^I < r_+^I < -r_-^I$	Plateau	{RW-I}	{RW-III}	{RW-II}	{DSW-VIII}	Plateau
$r_+^I > -r_-^I$	Plateau	{RW-II}	{RW-III}	{RW-II}	{DSW-VIII}	Plateau
$r_+^I = r_{A2}^{**}$	Plateau	{RW-I}	Plateau	{DSW-VIII}	Plateau	Null
$r_+^I = -r_-^I$	Plateau	{RW-I}	{RW-II}	{DSW-VIII}	Plateau	Null
$r_+^I = -r_-^I$	Plateau	{RW-III}	{RW-II}	{DSW-VIII}	Plateau	Null

Table 3 All of possible solution cases under condition A_3

Conditions	$-r_+^l < r_-^l$	$r_-^l = -r_+^l$	$-r_+^l < r_-^l < -r_+^l$	$r_-^l = -r_+^l$	$r_-^l < -r_+^l$
$-r_+^l < r_-^l \leq r_-^l$	$A_{3.11}$	Null	Null	Null	Null
$r_-^l = -r_+^l$	$A_{3.21}$	Null	Null	Null	Null
$-r_+^l < r_-^l < -r_+^l$	$A_{3.31}$	$A_{3.32}$	$A_{3.33}$	Null	Null
$r_-^l = -r_+^l$	$A_{3.41}$	$A_{3.42}$	$A_{3.43}$	Null	Null
$r_-^l < -r_+^l$	$A_{3.51}$	$A_{3.52}$	$A_{3.53}$	$A_{3.54}$	$A_{3.55}$

Table 4 Classification of solutions and region distributions for the subcases listed in Table 3 under condition A_3

Cases	Regions				
	Region 1	Region 2	Region 3	Region 4	Region 5
$A_{3,11}$	Plateau	{RW-II}	Plateau	{RW-I}	Plateau
$A_{3,21}$	Plateau	{RW-II}	{RW-I}	Plateau	Null
$A_{3,31}$	Plateau	{RW-II}	{RW-III}	{RW-I}	Plateau
$A_{3,41}$	Plateau	{RW-III}	{RW-I}	Plateau	Null
$A_{3,51}$	Plateau	{RW-I}	{RW-III}	{RW-I}	Plateau
$A_{3,32}$	Plateau	{RW-II}	{RW-III}	Plateau	Null
$A_{3,42}$	Plateau	{RW-III}	Plateau	Null	Null
$A_{3,52}$	Plateau	{RW-I}	{RW-III}	Plateau	Null
$A_{3,33}$	Plateau	{RW-II}	{RW-III}	{RW-II}	Plateau
$A_{3,43}$	Plateau	{RW-III}	{RW-II}	Plateau	Null
$A_{3,53}$	Plateau	{RW-I}	{RW-III}	{RW-II}	Plateau
$A_{3,54}$	Plateau	{RW-I}	{RW-II}	Plateau	Null
$A_{3,55}$	Plateau	{RW-I}	Plateau	{RW-II}	Plateau

(2) For $v_+(r_+^l, r_-^l) \leq x/t < v_+(-r_-^l, r_-^l)$, the solution is in the {RW-II} region with Riemann invariants

$$r_+ = -\frac{1}{5}r_-^l + \frac{1}{15}\sqrt{-36(r_-^l)^2 - 30 \cdot \frac{x}{t}}, \quad r_- = r_-^l.$$

(3) For $v_+(-r_-^l, r_-^l) \leq x/t < v_+(r_+^r, -r_+^r)$, the solution is in the {RW-III} region with Riemann invariants

$$r_+ = \frac{1}{\sqrt{6}}\sqrt{-\frac{x}{t}}, \quad r_- = -\frac{1}{\sqrt{6}}\sqrt{-\frac{x}{t}}.$$

(4) For $v_+(r_+^r, -r_+^r) \leq x/t < v_+(r_+^r, r_-^r)$, the solution is in the {RW-I} region with Riemann invariants

$$r_+ = r_+^r, \quad r_- = -\frac{1}{5}r_+^r - \frac{1}{15}\sqrt{-36(r_+^r)^2 - 30 \cdot \frac{x}{t}}.$$

(5) For $x/t \geq v_+(r_+^r, r_-^r)$, the solution is again in the plateau region with Riemann invariants

$$r_+ = r_+^r, \quad r_- = r_-^r.$$

Table 5 All of possible solution cases under condition B_1

Conditions	$r_+^r < r_{B_1}^*$	$r_+^r = r_{B_1}^*$	$r_{B_1}^* < r_+^r < r_{B_1}^{**}$	$r_+^r = r_{B_1}^{**}$	$r_+^r > r_{B_1}^{**}$
$r_+^l < r_{B_1}^*$	$B_{1.11}$	Null	Null	Null	Null
$r_+^l = r_{B_1}^*$	$B_{1.21}$	Null	Null	Null	Null
$r_{B_1}^* < r_+^l < r_{B_1}^{**}$	$B_{1.31}$	$B_{1.32}$	$B_{1.33}$	Null	Null
$r_+^l = r_{B_1}^{**}$	$B_{1.41}$	$B_{1.42}$	$B_{1.43}$	Null	Null
$r_+^l > r_{B_1}^{**}$	$B_{1.51}$	$B_{1.52}$	$B_{1.53}$	$B_{1.54}$	$B_{1.55}$

4.2 Case B. $r_+^l > r_+^r > r_-^l > r_-^r$

This is a particular case in which certain exotic phenomena of wave breakings are demonstrated. The vertex r_{BCD}^* of the parabolas connecting Riemann invariants λ_2 with λ_3 plays a vital role in the classification of the solution for the Riemann problem in Case B, where r_{BCD}^* solves

$$\frac{\partial v_3(r_+^r, r_{BCD}^*, r_{BCD}^*, r_-^r)}{\partial r_B^*} = 0, \tag{91}$$

from which one has $r_{BCD}^* = -\frac{1}{4}(r_+^r + r_-^r)$. In viewing Fig. 4 and its descriptions, it is observed that there are several subcases in Case B (also in Cases C and D).

4.2.1 Subcase B_1 : $r_-^l \leq r_{BCD}^*$ and $r_+^r > r_{BCD}^*$

Similar to case A_1 , there also exist many subcases in B_1 , where a new basic dispersive shock wave structure {DSW-IX} emerges. The classification of almost all subcases in B_1 are display in Table 5, in which $r_{B_1}^* = -\frac{1}{3}r_-^r - \frac{2}{3}r_-^l$ solves

$$v_1(r_{B_1}^*, r_-^l, r_-^l, r_-^r) = v_3(r_{B_1}^*, r_-^l, r_-^l, r_-^r), \tag{92}$$

and $r_{B_1}^{**} = r_-^r - r_-^l + \sqrt{5(r_-^r)^2 - 4r_-^l r_-^r}$ solves

$$v_1(r_{B_1}^{**}, r_-^l, r_-^r, r_-^r) = v_3(r_{B_1}^{**}, r_-^l, r_-^r, r_-^r). \tag{93}$$

The classification of solutions and region distributions for the subcases listed in Table 5 are given in Table 6. It is remarked that except case $B_{1.42}$, which is in fact one of the basic rarefaction wave structures of {DSW-IX} displayed in Fig. 5 (and there exists only three regions), all cases evolve at least four regions, and in each case, the boundary velocities can be given easily.

In what follows, only case $B_{1.33}$ is discussed in details, see also Fig. 9, where the initial conditions for Riemann invariants are chosen to be $r_+^l = 1, r_+^r = 0.8, r_-^l = -0.5, r_-^r = -1$. So one has $r_{B_1}^* = 0.6$ and $r_{B_1}^{**} = \sqrt{3} - \frac{1}{2}$. Figure 9 demonstrates the

Table 6 Classification of solutions and region distributions for the subcases listed in Table 5 under condition B_1

Cases	Regions				
	Region 1	Region 2	Region 3	Region 4	Region 5
$B_{1.11}$	Plateau	{DSW-I}	Plateau	{RW-II}	Plateau
$B_{1.21}$	Plateau	{DSW-I}	{RW-II}	Plateau	Null
$B_{1.31}$	Plateau	{DSW-I}	{DSW-IX}	{RW-II}	Plateau
$B_{1.41}$	Plateau	{DSW-IX}	{RW-II}	Plateau	Null
$B_{1.51}$	Plateau	{RW-II}	{DSW-IX}	{RW-II}	Plateau
$B_{1.32}$	Plateau	{DSW-I}	{DSW-IX}	Plateau	Null
$B_{1.42}$	Plateau	{DSW-IX}	Plateau	Null	Null
$B_{1.52}$	Plateau	{RW-II}	{DSW-IX}	Plateau	Null
$B_{1.33}$	Plateau	{DSW-I}	{DSW-IX}	{DSW-I}	Plateau
$B_{1.43}$	Plateau	{DSW-IX}	{DSW-I}	Plateau	Null
$B_{1.53}$	Plateau	{RW-II}	{DSW-IX}	{DSW-I}	Plateau
$B_{1.54}$	Plateau	{RW-II}	{DSW-I}	Plateau	Null
$B_{1.55}$	Plateau	{RW-II}	Plateau	{DSW-I}	Plateau

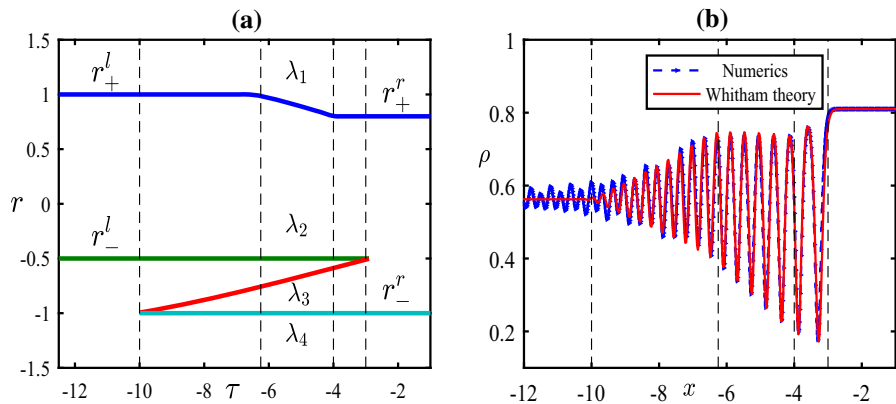


Fig. 9 (Color online) Example of the self-similar solution for case $B_{1.33}$ with initial condition $r_+^l = 1, r_+^r = 0.8, r_-^l = -0.5, r_-^r = -1$ at time $t = 1$: **a** distributions of the Riemann invariants in five regions; **b** comparison of the analytical solution from Whitham modulation theory (solid red line) with direct numerical simulations (dash blue line)

distributions of the Riemann invariants and the comparison of the analytical solution from Whitham modulation theory with direct numerical simulations. It is observed that the three middle regions form a larger genus-1 dispersive shock wave consisting of three genus-1 DSWs, in which an exotic DSW structure {DSW-IX} is evolved. The boundaries of those regions are separated by four black dotted lines, see Fig. 9a, which is quite different from the structures of wave breaking in the oscillation region observed before (Kodama et al. 2008). Moreover, Fig. 9b shows that the analytical result from Whitham modulation theory agrees well with the direct numerical simulations.

In case $B_{1,33}$, the solution of the Riemann invariants consists of five regions (see Fig. 9a), and in each region, the Riemann invariants can be formulated below.

- (1) For $x/t \leq v_3(r_+^l, r_-^l, r_-^r, r_-^r)$, the solution is in the plateau region with Riemann invariants

$$r_+ = r_+^l, \quad r_- = r_-^l.$$

- (2) For $v_3(r_+^l, r_-^l, r_-^r, r_-^r) < x/t < v_1(r_+^l, r_-^l, r_{Be}^*, r_-^r)$, where r_{Be}^* solves $v_1(r_+^l, r_-^l, r_{Be}^*, r_-^r) = v_3(r_+^l, r_-^l, r_{Be}^*, r_-^r)$ and locates in the interval $[r_-^r, r_-^l]$, the solution is in the {DSW-I} region with Riemann invariants

$$\lambda_1 = r_+^l, \quad \lambda_2 = r_-^l, \quad \frac{x}{t} = v_3(r_+^l, r_-^l, \lambda_3, r_-^r), \quad \lambda_4 = r_-^r.$$

- (3) For $v_1(r_+^l, r_-^l, r_{Be}^{**}, r_-^r) \leq x/t < v_3(r_+^r, r_-^l, r_{Be}^{**}, r_-^r)$, where r_{Be}^{**} satisfies $v_1(r_+^r, r_-^l, r_{Be}^{**}, r_-^r) = v_3(r_+^r, r_-^l, r_{Be}^{**}, r_-^r)$ located in the interval $[r_-^r, r_-^l]$, the solution is in the {DSW-IX} region with Riemann invariants

$$\frac{x}{t} = v_1(\lambda_1, r_-^l, \lambda_3, r_-^r), \quad \lambda_2 = r_-^l, \quad \frac{x}{t} = v_3(\lambda_1, r_-^l, \lambda_3, r_-^r), \quad \lambda_4 = r_-^r.$$

- (4) For $v_3(r_+^r, r_-^l, r_{Be}^{**}, r_-^r) \leq x/t < v_3(r_+^r, r_-^l, r_-^r, r_-^r)$, the solution is in the {DSW-I} region with Riemann invariants

$$\lambda_1 = r_+^r, \quad \lambda_2 = r_-^l, \quad \frac{x}{t} = v_3(r_+^r, r_-^l, \lambda_3, r_-^r), \quad \lambda_4 = r_-^r.$$

- (5) For $x/t \geq v_3(r_+^r, r_-^l, r_-^r, r_-^r)$, the solution is in the plateau region with Riemann invariants

$$r_+ = r_+^r, \quad r_- = r_-^l.$$

The boundary velocities $x/t = v_3(r_+^l, r_-^l, r_-^r, r_-^r)$ and $x/t = v_3(r_+^r, r_-^l, r_-^r, r_-^r)$ are known as trailing edge and leading edge, respectively. The Riemann invariants match at the boundaries of zero-phase solution region and one-phase solution region, see below.

At the trailing edge, i.e., harmonic front with $\lambda_3 = \lambda_4$ and $m = 0$ (see Eq. 55), we have

$$(\lambda_1, \lambda_2) = \text{the rarefaction wave solution outside the oscillation region.}$$

At leading edge, i.e., soliton front with $\lambda_3 = \lambda_2$ and $m = 0$ (see Eq. 55), we have

$$(\lambda_1, \lambda_4) = \text{the rarefaction wave solution outside the oscillation region.}$$

Table 7 Classification of solutions and region distributions for the subcases listed in Table 5 under condition B_2

Cases	Regions					
	Region 1	Region 2	Region 3	Region 4	Region 5	Region 6
$B_{2.1}$	Plateau	{DSW-I}	{DSW-IX}	{DSW-I}	{DSW-V}	Plateau
$B_{2.2}$	Plateau	{RW-II}	{DSW-I}	{DSW-V}	Plateau	Null
$B_{2.3}$	Plateau	{RW-II}	Plateau	{DSW-I}	{DSW-V}	Plateau
$B_{2.4}$	Plateau	{RW-II}	Plateau	{DSW-V}	Plateau	Null
$B_{2.5}$	Plateau	{RW-II}	Plateau	{RW-I}	{DSW-V}	Plateau

4.2.2 Subcase B_2 : $r_-^l > r_{BCD}^*$ and $r_-^r < r_{BCD}^*$

Taking $r_{B_2}^* = r_-^r - r_-^l + \sqrt{5(r_-^r)^2 - 4r_-^l r_-^r}$, the complete classification under condition B_2 is given below:

For $r_-^l < r_{B_2}^*$, there are three cases as follows

- $B_{2.1}$: $r_+^r < r_{B_2}^*$, $r_+^l < r_{B_2}^*$.
- $B_{2.2}$: $r_+^r = r_{B_2}^*$, $r_+^l > r_{B_2}^*$.
- $B_{2.3}$: $r_+^r > r_{B_2}^*$, $r_+^l > r_{B_2}^*$.

For $r_-^l = r_{B_2}^*$, there is only one case

- $B_{2.4}$: $r_+^r > r_{B_2}^*$, $r_+^l > r_{B_2}^*$.

For $r_-^l > r_{B_2}^*$, there is also only one case

- $B_{2.5}$: $r_+^r > r_{B_2}^*$, $r_+^l > r_{B_2}^*$.

The classification of solutions and region distributions for these subcases are given in Table 7. It is shown that all cases evolve at least five regions, in which the exotic DSW structure {DSW-IX} appears again.

In the following, the case $B_{2.1}$ is taken as an example to exhibit the novel wave breaking appearing under the condition B_2 . Figure 10 demonstrates the distributions of the Riemann invariants and the comparison of the analytical solution from Whitham modulation theory with direct numerical simulations. It is seen that the four middle regions form a larger genus-1 dispersive shock wave consisting of four genus-1 DSWs, which definitely does not appear under condition B_1 . The boundaries of those regions are separated by five black dotted lines, see Fig. 10a, which has not been found before (Kodama et al. 2008). It is also found from Fig. 10b that the analytical result from Whitham modulation theory agrees well with the direct numerical simulations. In fact, the fourth and fifth regions for case $B_{2.1}$ shown in Fig. 10 is generated by dividing the fourth region in case $B_{1.33}$ displayed in Fig. 9. Thus only the boundary velocities of the fifth region, i.e., the {DSW-VI} region, is proposed below and the other regions are the same as case $B_{1.33}$.

For the {DSW-VI} region in Fig. 10, the Riemann invariants are

$$\lambda_1 = r_+^r, \quad \frac{x}{t} = v_2(r_+^r, \lambda_2, \lambda_3, r_-^r), \quad \frac{x}{t} = v_3(r_+^r, \lambda_2, \lambda_3, r_-^r), \quad \lambda_4 = r_-^r, \quad (94)$$

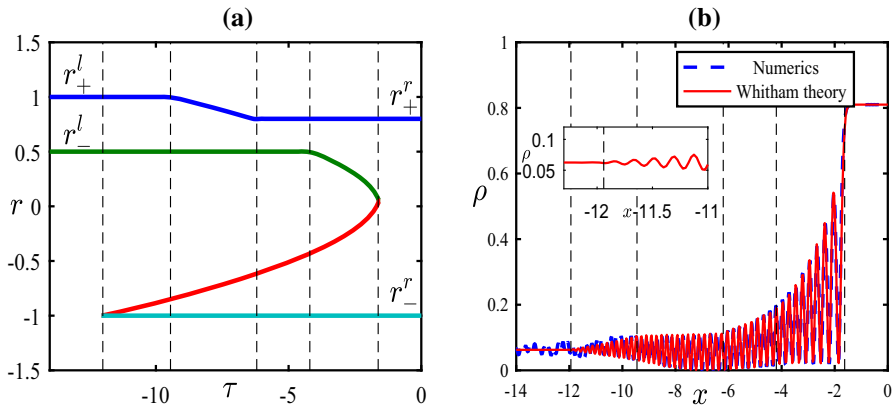


Fig. 10 (Color online) Example of the self-similar solution for case $B_{2,1}$ with initial conditions $r_+^l = 1, r_+^r = 0.8, r_-^l = 0.5, r_-^r = -1$ at time $t = 1$: **a** distributions of the Riemann invariants in five regions; **b** comparison of the analytical solution from Whitham modulation theory (solid red line) with direct numerical simulations (dash blue line)

for $v_2(r_+^r, r_-^l, r_{Be}^{**}, r_-^r) < x/t \leq v_3(r_+^r, r_{Be}^*, r_{Be}^*, r_-^l)$, where $r_{Be}^* = r_B^* = -\frac{1}{4}(r_+^r + r_-^l)$ and r_{Be}^{**} satisfies an implicit equation

$$v_2(r_+^r, r_-^l, r_{Be}^{**}, r_-^r) = v_3(r_+^r, r_-^l, r_{Be}^*, r_-^r). \tag{95}$$

In particular, it can be calculated that $r_{Be}^* = r_B^* = 0.05$ and $r_{Be}^{**} \approx -0.4195$ in case $B_{2,1}$ with the initial conditions $r_+^l = 1, r_+^r = 0.8, r_-^l = 0.5, r_-^r = -1$.

4.2.3 Subcase $B_3: r_-^r \geq r_{BCD}^*$

The condition $r_-^r \geq r_B^*$ indicates $r_-^r \geq -\frac{1}{3}r_+^r$ which only produces rarefaction waves, see Sect. 3.1 for details. Thus the solution regions in this case only consist of plateau, {RW-II}, plateau, {RW-I}, plateau. Figure 11 displays the distributions of the Riemann invariants and the comparison of the analytical solution from Whitham modulation theory with direct numerical simulations, which shows that the result of Whitham modulation theory agrees well with the direct numerical simulations.

4.2.4 Subcase $B_4: r_+^l < r_{BCD}^*$

In this case, the four initial values r_+^l, r_+^r, r_-^l and r_-^r are all below the critical point r_B^* . Define four critical points $r_{B_4}^*, r_{B_4}^{**}, rr_{B_4}^*$ and $rr_{B_4}^{**}$ in the following way:

- Let $r_{B_4}^* \in [r_+^r, r_+^l]$ solve the implicit equation $v_1(r_{B_4}^*, r_+^r, r_+^l, r_-^r) = v_2(r_{B_4}^*, r_+^r, r_+^l, r_-^r)$.
- Let $r_{B_4}^{**} \in [r_+^r, r_+^l]$ satisfy equation $\partial v_1(r_{B_4}^{**}, r_{B_4}^{**}, r_+^r, r_-^l) / \partial r_{B_4}^{**} = 0$.
- Let $rr_{B_4}^* \in [r_{B_4}^*, r_+^l]$ solve the implicit equation $v_1(rr_{B_4}^*, r_-^l, r_-^l, r_-^r) = v_3(rr_{B_4}^*, r_-^l, r_-^l, r_-^r)$.

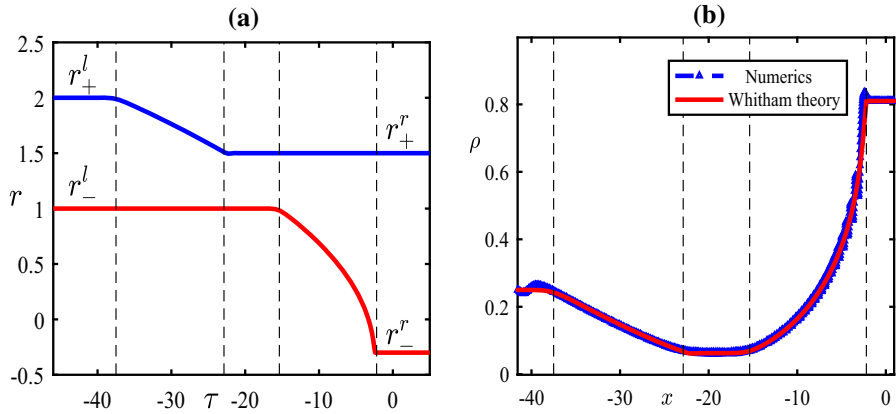


Fig. 11 (Color online) Examples of self-similar solutions of of case B_3 with initial condition $r_+^l = 2, r_+^r = 1.5, r_-^l = 1, r_-^r = -0.3$ at time $t = 1$: **a** distributions of Riemann invariants; **b** comparison of numerical simulation (dash blue line) with analytical solution (solid red line) of the defocusing cmKdV equation (1)

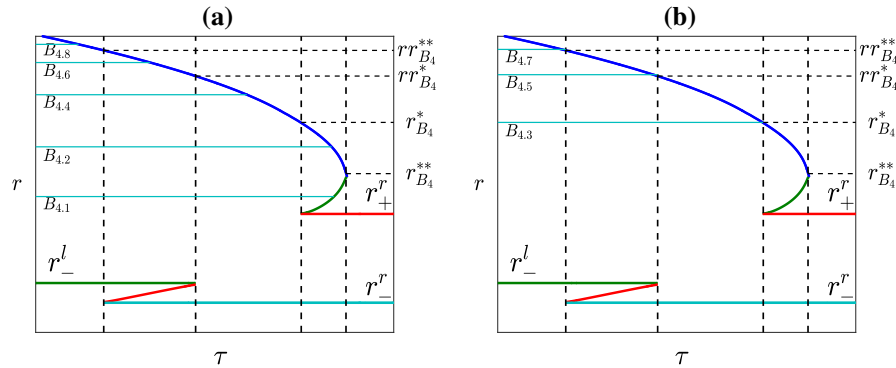


Fig. 12 (Color online) Distributions of Riemann invariants for all the possible cases in Case B_4 : **a** the characteristic velocity r_+^l is chosen to divide the corresponding region into two smaller regions; **b** the characteristic velocity r_+^l is chosen to equal to the boundary velocities $r_{B_4}^*, r_{B_4}^{**}, rr_{B_4}^*$ and $rr_{B_4}^{**}$

- Let $rr_{B_4}^{**}$ solve the implicit equation $v_1(rr_{B_4}^{**}, r_-^l, r_-^r) = v_3(rr_{B_4}^{**}, r_-^l, r_-^r)$.

The complete classification of case B_4 can be given by adjusting the initial value r_+^l , which is, more or less, similar to case A_1 and is described in Fig. 12.

The classification of solutions and region distributions for the subcases in Fig. 12 are given in Table 8, which shows that all cases evolve at least five regions. It is worth mentioning that three DSWs are separated by a plateau in case $B_{4.2}$, two DSWs are separated by a plateau and a rarefaction wave in case $B_{4.4}$, and three DSWs are separated by a rarefaction wave in case $B_{4.6}$. These are the main features in case B_4 .

We only take case $B_{4.4}$ as an example to exhibit the phenomena of wave breaking under the condition B_2 . Figure 13 shows that the solution for case $B_{4.4}$ consists of six regions with two different patterns of the oscillating DSWs separated by a plateau and a rarefaction wave, in which the left oscillating pattern corresponding to {DSW-I} and

Table 8 Classification of solutions and region distributions for the subcases listed in Table 5 under condition B_4

Cases	Regions					
	Region 1	Region 2	Region 3	Region 4	Region 5	Region 6
$B_{4.1}$	Plateau	{DSW-I}	Plateau	{DSW-IV}	Plateau	Null
$B_{4.2}$	Plateau	{DSW-I}	Plateau	{DSW-IV}	{DSW-VIII}	Plateau
$B_{4.3}$	Plateau	{DSW-I}	Plateau	{DSW-VIII}	Plateau	Null
$B_{4.4}$	Plateau	{DSW-I}	Plateau	{RW-II}	{DSW-VIII}	Plateau
$B_{4.5}$	Plateau	{DSW-I}	{RW-II}	{DSW-VIII}	Plateau	Null
$B_{4.6}$	Plateau	{DSW-I}	{DSW-IX}	{RW-II}	{DSW-VIII}	Plateau
$B_{4.7}$	Plateau	{DSW-IX}	{RW-II}	{DSW-VIII}	Plateau	Null
$B_{4.8}$	Plateau	{RW-II}	{DSW-IX}	{RW-II}	{DSW-VIII}	Plateau

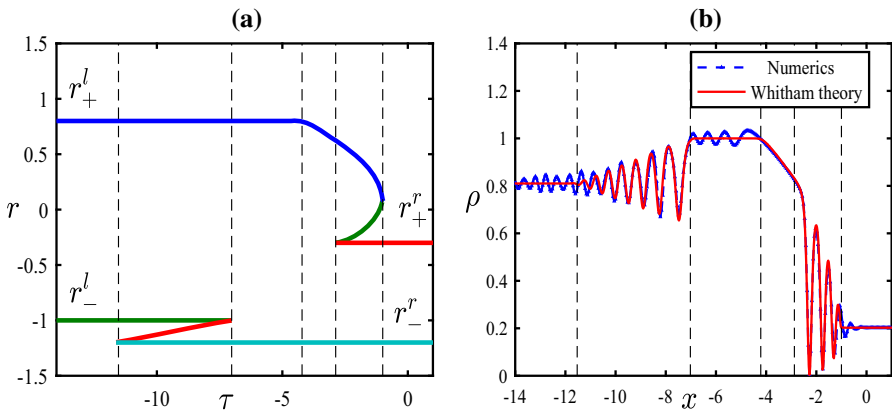


Fig. 13 (Color online) Example of self-similar solution of case $B_{4.4}$ with initial condition $r_+^l = 0.8, r_+^r = -0.3, r_-^l = -1, r_-^r = -1.2$ at time $t = 1$: **a** distributions of Riemann invariants; **b** comparison of numerical simulation (dash blue line) with analytical solution (solid red line) of the defocusing cmKdV equation (1)

the right pattern corresponding to {DSW-VIII}. Figure 13b indicates that the result of Whitham modulation theory agrees well with the direct numerical simulations. The boundary velocities in each region are given below.

- (1) For $x/t \leq v_3(r_+^l, r_-^l, r_-^r, r_-^r)$, the solution is in the plateau region with Riemann invariants

$$r_+ = r_+^l, \quad r_- = r_-^l.$$

- (2) For $v_3(r_+^l, r_-^l, r_-^r, r_-^r) < x/t < v_3(r_+^l, r_-^l, r_-^r, r_-^r)$, the solution is in the {DSW-I} region with Riemann invariants

$$\lambda_1 = r_+^l, \quad \lambda_2 = r_-^l, \quad \frac{x}{t} = v_3(r_+^l, r_-^l, \lambda_3, r_-^r), \quad \lambda_4 = r_-^r.$$

- (3) For $v_3(r_+^l, r_-^l, r_-^l, r_-^r) \leq x/t \leq v_1(r_+^l, r_+^r, r_+^r, r_-^r)$, the solution is in the plateau region with Riemann invariants

$$r_+ = r_+^l, \quad r_- = r_-^r.$$

- (4) For $v_1(r_+^l, r_+^r, r_+^r, r_-^r) < x/t < v_1(r_{B4}^*, r_+^r, r_+^r, r_-^r)$, the solution is in the {RW-II} region with Riemann invariants

$$r_+ = -\frac{1}{5}r_-^r + \frac{1}{15}\sqrt{-36(r_-^r)^2 - 30 \cdot \frac{x}{t}}, \quad r_- = r_-^r.$$

- (5) For $v_1(r_{B4}^*, r_+^r, r_+^r, r_-^r) \leq x/t \leq v_1(r_{B4}^{**}, r_{B4}^{**}, r_+^r, r_-^r)$, the solution is in the {DSW-VIII} region with Riemann invariants

$$\frac{x}{t} = v_1(\lambda_1, \lambda_2, r_+^r, r_-^r), \quad \frac{x}{t} = v_2(\lambda_1, \lambda_2, r_+^r, r_-^r), \quad \lambda_3 = r_+^r, \quad \lambda_4 = r_-^r.$$

- (6) For $x/t > v_1(r_{B4}^{**}, r_{B4}^{**}, r_+^r, r_-^r)$, the solution is again in the plateau region with Riemann invariants

$$r_+ = r_+^r, \quad r_- = r_-^r.$$

Notice that the directions of leading and trailing edges of two DSWs in Fig. 13 are opposite.

4.3 Case C. $r_+^l > r_-^l > r_+^r > r_-^r$

This is an special case, in which the vacuum region and genus-2 region appear. The vertex r_{BCD}^* in equation (91) is a vital point in classifying the solution of the Riemann problem in Case C. In what follows, the subcase that only rarefaction wave emerges is discussed firstly.

4.3.1 Subcase $C_1: r_-^r \geq r_{BCD}^*$

This case only contains one class of solution, where one vacuum and two rarefaction waves are produced. Figure 14 shows that the solution for case C_1 consists of five regions, where two different patterns of rarefaction waves are separated by a vacuum, see also Table 10. Figure 14b indicates that the result of Whitham modulation theory agrees well with the direct numerical simulations. The formation of these profiles is much similar to the case under B_3 except the intermediate plateau connecting the two rarefaction waves is replaced with the vacuum region. This result can also be observed in the Riemann problem of the defocusing NLS equation (El et al. 1995). The boundary velocities in this case is omitted since it can also be easily derived in the same way.

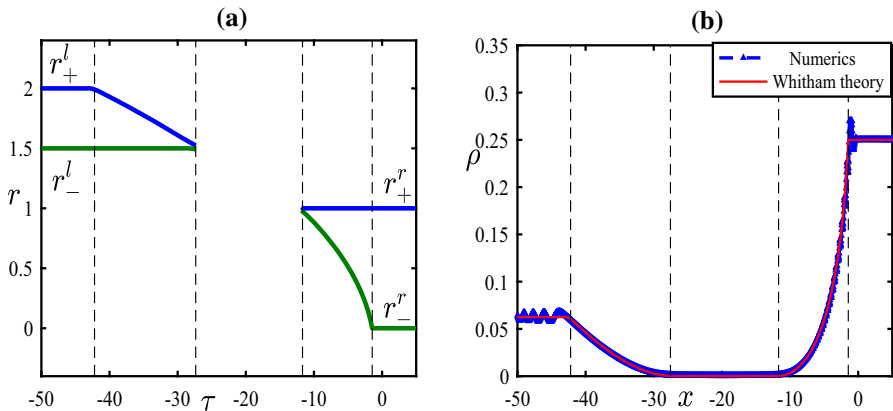


Fig. 14 (Color online) Example of the self-similar solution of case C_1 with initial condition $r_+^l = 2, r_+^r = 1, r_-^l = 1.5, r_-^r = 0$ at time $t = 1$: **a** distributions of Riemann invariants; **b** comparison of numerical simulation (dash blue line) with analytical solution (solid red line) of the defocusing cmKdV equation (1)

Table 9 All of possible solution cases under conditions C_1 and C_2

Conditions	$r_-^r \geq r_{BCD}^*$	$r_{C_2}^* < r_-^r < r_{BCD}^*$	$r_-^r = r_{C_2}^*$	$-r_-^l < r_-^r < r_{C_2}^*$
Cases	C_1	$C_{2.1}$	$C_{2.2}$	$C_{2.3}$
Conditions	$r_-^r = -r_-^l$	$-r_+^l < r_-^r < -r_-^l$	$r_-^r = -r_+^l$	$r_-^r < -r_+^l$
Cases	$C_{2.4}$	$C_{2.5}$	$C_{2.6}$	$C_{2.7}$

4.3.2 Subcase C_2 : $r_+^r > r_{BCD}^*$ and $r_-^r < r_{BCD}^*$

The inequality $r_-^r < r_{BCD}^*$ indicates that $r_-^r < -\frac{1}{5}r_+^r$, which provides a condition of producing DSW. The complete classification under condition C_2 can be obtained by adjusting the value of r_-^r in comparison with r_{BCD}^* and $r_{C_2}^* = r_+^r - r_-^r - \sqrt{5(r_+^r)^2 - 4r_+^r r_-^r}$, see Table 9.

The classification of solutions and region distributions for the subcases listed in Table 9 are given in Table 10. It is observed that there are plateau, vacuum, rarefaction waves, and DSW in case $C_{2.3}$, which will be displayed in Fig. 15 below. Moreover, in cases $C_{2.5} - C_{2.7}$ there exist oscillatory regions, which are also genus-1 DSW regions but they do not belong to any basic structures of DSW shown in Sect. 3.2. Notice that oscillatory region is a bit similar to the region that found in El et al. (1995), in which the amplitude of the oscillation is a constant ($a = 0$) there. However, different from the results in El et al. (1995) the oscillation in this work is a variable. It seen in the oscillatory region that $a \rightarrow 0$ when $\lambda_3 \rightarrow \lambda_4$ in the left hand side, or $\lambda_1 \rightarrow \lambda_2$ in the right hand side. This implies that the left half part of oscillatory region can be interpreted as the trailing edge of {DSW-IX} and the symmetry with respect to vertical axis of trailing edge of {DSW-X} for the right part.

Table 10 Classification of solutions and region distributions for the subcases listed in Table 5 under condition C_2

Cases	Regions					
	Region 1	Region 2	Region 3	Region 4	Region 5	Region 6
C_1	Plateau	{RW-II}	Vacuum	{RW-I}	plataeu	Null
$C_{2.1}$	Plateau	{RW-II}	Vacuum	{RW-I}	{DSW-VI}	Plateau
$C_{2.2}$	Plateau	{RW-II}	Vacuum	{DSW-VI}	plataeu	Null
$C_{2.3}$	Plateau	{RW-II}	Vacuum	{RW-V}	{DSW-VI}	Plateau
$C_{2.4}$	Plateau	{RW-II}	{RW-V}	{DSW-VI}	plataeu	Null
$C_{2.5}$	Plateau	{RW-II}	Oscillation	{RW-V}	{DSW-VI}	Plateau
$C_{2.6}$	Plateau	Oscillation	{RW-V}	{DSW-VI}	Plateau	Null
$C_{2.7}$	Plateau	{DSW-I}	Oscillation	{RW-V}	{DSW-VI}	Plateau

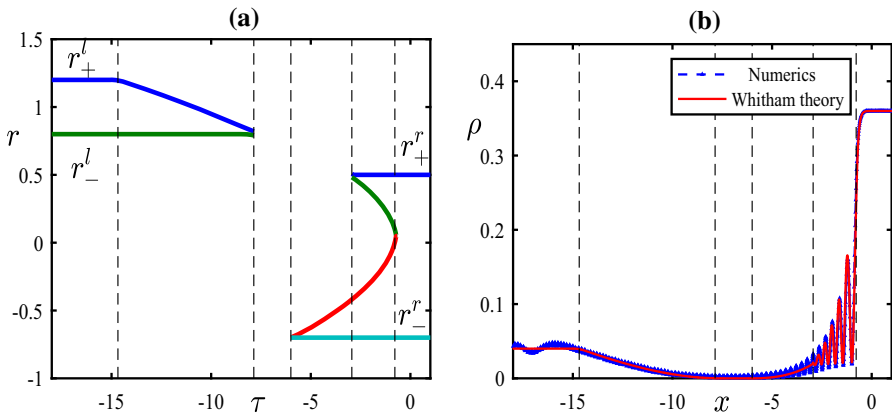


Fig. 15 (Color online) Example of the self-similar solution of case $C_{2.3}$ with initial condition $r_+^l = 1.2, r_+^r = 0.5, r_-^l = 0.8, r_-^r = -0.7$ at time $t = 1$: **a** distributions of Riemann invariants; **b** comparison of numerical simulation (dash blue line) with analytical solution (solid red line) of the defocusing cmKdV equation (1)

Figure 15 shows that the solution for case $C_{2.3}$ with initial condition $r_+^l = 1.2, r_+^r = 0.5, r_-^l = 0.8, r_-^r = -0.7$ consists of six regions including plateau, vacuum, rarefaction waves and DSW. Figure 15b indicates that the analytical solution from Whitham modulation theory agrees well with the direct numerical simulations. From left to right, the fourth region is a rarefaction wave followed from equation (57), where

$$v_3|_{\lambda_1=\lambda_2} = -\frac{15}{2}r_3^2 - 3r_4r_3 - \frac{3}{2}r_4^2, \quad v_4|_{\lambda_1=\lambda_2} = -\frac{3}{2}r_3^2 - 3r_4r_3 - \frac{15}{2}r_4^2.$$

The fifth region, the dispersive shock wave region, can be regard as the limitation state of {DSW-VI} for $\lambda_2 \rightarrow \lambda_3$.

4.3.3 Subcase $C_3: r_+^r \leq r_{BCD}^*$

The condition $r_+^r \leq r_{BCD}^*$ shows that $r_+^r \leq -\frac{1}{5}r_-^r$ which will result in the collision of two DSWs as seen in Fig. 13. Moreover, in this case, certain region can not be described by the genus-1 Whitham equations (56) with (57) definitely. Thus the genus-2 regions may emerge, which should be analyzed by the genus-2 Whitham equations (64) with (66). The initial condition of Fig. 16 is $r_+^l = 0, r_+^r = -0.8, r_-^l = -0.5, r_-^r = -1.2$. It is shown that the solution for case C_3 consists of five regions with two different genus-1 DSWs separated by a genus-2 DSW. Fig. 16b demonstrates the result of direct numerical simulations, which displays that the middle genus-2 DSW region oscillates rapidly, which further verifies the result of Whitham modulation theory shown in Fig. 16a. The boundaries of the genus-2 DSW region are $x = s_1t$ and $x = s_2t$ with $s_1 = -7.3$ and $s_2 = -4.5$. In fact, s_1 and s_2 are characteristic velocities obtained by the genus-2 Whitham equations (64) with (66). The new feature of middle genus-2 DSW region can be explained as follows: Two genus-1 dispersive shock waves (genus-1 undular bores) move toward each other and overlap in region $[s_1, s_2]$ to generate a genus-2 dispersive shock wave that can be described by the two-phase solution of the defocusing cmKdV equation (1).

This work does not present the detailed description of the genus-2 DSW region but give the appropriate solution for the genus-2 averaged Whitham equation

$$\frac{\partial \lambda_i}{\partial t} + v_i(\lambda_1, \lambda_2, \lambda_3, \lambda_4, \lambda_5, \lambda_6) \frac{\partial \lambda_i}{\partial x} = 0, \quad i = 1, 2, \dots, 6,$$

where $\lambda_1 > \lambda_2 > \lambda_3 > \lambda_4 > \lambda_5 > \lambda_6$. The self-similar solution of this equation in the region $[s_1, s_2]$ is expressed by

$$\begin{aligned} \lambda_1 &= r_+^l, \quad \lambda_2 = r_-^l, \quad \lambda_5 = r_+^r, \quad \lambda_6 = r_-^r, \\ v_3(r_+^l, r_-^l, \lambda_3, \lambda_4, r_+^r, r_-^r) &= \tau = v_4(r_+^l, r_-^l, \lambda_3, \lambda_4, r_+^r, r_-^r), \end{aligned}$$

from which the the boundary characteristic velocities s_1 and s_2 are

$$s_1 = v_3(r_+^l, r_-^l, \lambda_3^*, r_+^r, r_-^r, r_-^r), \quad s_2 = v_4(r_+^l, r_-^l, r_-^l, \lambda_4^*, r_+^r, r_-^r).$$

4.4 Case D. $r_+^r > r_+^l > r_-^l > r_-^r$

More genus-2 DSW regions emerge in this case because of the collisions of the DSWs. As before, the vertex r_{BCD}^* in equation (91) is still an important point in classifying the solution of the Riemann problem for Case D.

4.4.1 Subcase $D_1: r_-^l > r_{BCD}^*$

The genus-2 DSW region also appears due to the collision of {DSW-II} and {DSW-V} under condition D_1 . Since the genus-2 DSWs are more complicated than the genus-1

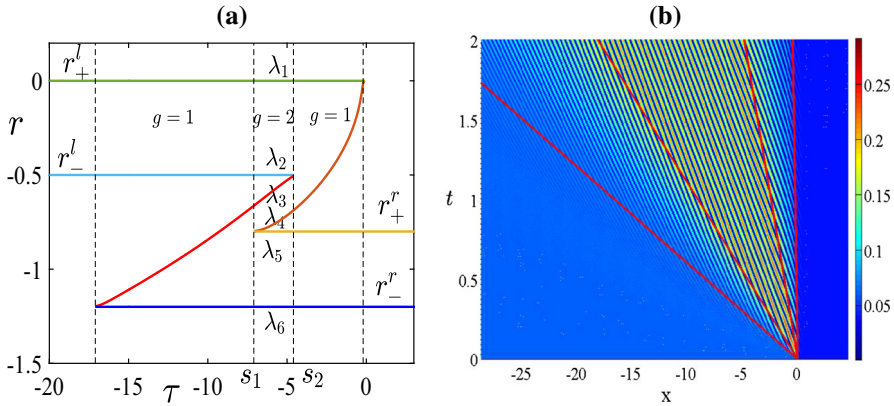


Fig. 16 (Color online) Example of the self-similar solution of case C_3 with initial condition $r_+^l = 0, r_+^r = -0.8, r_-^l = -0.5, r_-^r = -1.2$: **a** distributions of Riemann invariants; **b** direct numerical simulation, where the red lines represent the boundary of each region corresponding to the black dotted line in **a**

Table 11 All of possible solution cases under condition D_1

Conditions	$r_-^r \geq r_{BCD}^*$	$r_{D_1}^* < r_-^r < r_{BCD}^*$	$r_-^r = r_{D_1}^*$	$r_{D_1}^{**} < r_-^r < r_{D_1}^*$
Cases	$D_{1.1}$	$D_{1.2}$	$D_{1.3}$	$D_{1.4}$
Conditions	$r_-^r = r_{D_1}^{**}$	$r_{D_1}^{***} < r_-^r < r_{D_1}^{**}$	$r_-^r = r_{D_1}^{***}$	$r_-^r < r_{D_1}^{***}$
Cases	$D_{1.5}$	$D_{1.g2}$	$D_{1.g2}$	$D_{1.g2}$

DSWs, this work only gives the classification cases under condition D_1 and lists the solution regions only including genus-1 DSWs; see Tables 11 and 12, respectively. Define three critical points $r_{D_1}^*, r_{D_1}^{**}$ and $r_{D_1}^{***}$ in the following way:

- Let $r_{D_1}^*$ solve the implicit equation $v_2(r_+^r, r_-^l, r_{D_1}^*, r_-^r) = v_3(r_+^r, r_-^l, r_{D_1}^*, r_-^r)$.
- Let $r_{D_1}^{**}$ solve the implicit equation $v_2(r_+^r, r_+^l, r_+^l, r_-^l) = v_3(r_+^r, r_-^l, r_{D_1}^{**}, r_{D_1}^{**})$ on the interval $(-\infty, r_{D_1}^*)$.
- Let $r_{D_1}^{***}$ solve the implicit equation $v_2(r_+^r, r_+^r, r_+^l, r_-^l) = v_3(r_+^r, r_+^l, r_{D_1}^{***}, r_{D_1}^{***})$ on the interval $(-\infty, r_{D_1}^{**})$.

The complete classification of case D_1 can be given by adjusting the initial value r_-^r , which is described in Table 11. The region remarked by $D_{1.g2}$ is the place where the genus-2 region appears. The classification of solutions and region distributions for the subcases $D_{1.1}$ - $D_{1.5}$ in Table 11 are given in Table 12.

We only take case $D_{1.2}$ as an example to exhibit the phenomena of wave breaking under the condition D_1 . Figure 17 shows that the solution for case $D_{1.2}$ consists of six regions with two different patterns of the oscillating DSWs separated by a plateau and a rarefaction wave. Figure 17b indicates that the analytical result of Whitham theory agrees well with the direct numerical simulations.

Table 12 Classification of solutions and region distributions for the subcases $D_{1,1}$ - $D_{1,5}$ listed in Table 11 under condition D_1

Cases	Regions					
	Region 1	Region 2	Region 3	Region 4	Region 5	Region 6
$D_{1,1}$	Plateau	{DSW-II}	Plateau	{RW-IV}	Plateau	Null
$D_{1,2}$	Plateau	{DSW-II}	Plateau	{RW-IV}	{DSW-V}	Plateau
$D_{1,3}$	Plateau	{DSW-II}	Plateau	{DSW-V}	Plateau	Null
$D_{1,4}$	Plateau	{DSW-II}	Plateau	{RW-I}	{DSW-V}	Plateau
$D_{1,5}$	Plateau	{DSW-II}	{RW-I}	{DSW-V}	Plateau	Null

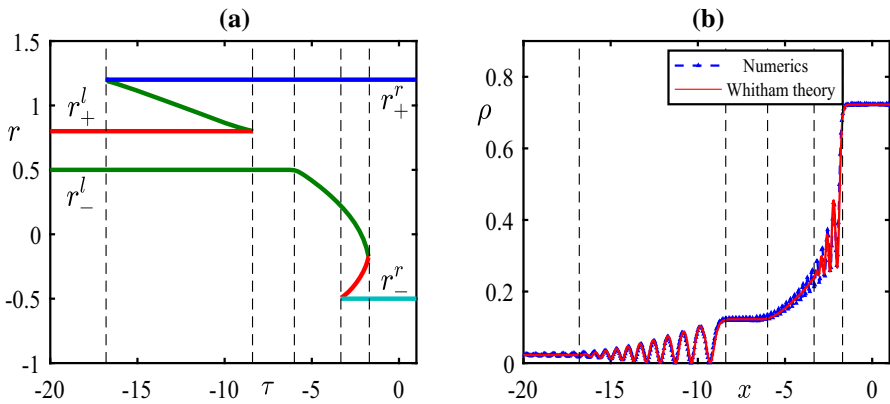


Fig. 17 (Color online) Example of self-similar solution of case $D_{1,2}$ with initial condition $r_+^l = 0.8$, $r_+^r = 1.2$, $r_-^l = 0.5$, $r_-^r = -0.5$ at time $t = 1$: **a** distributions of Riemann invariants; **b** comparison of numerical simulation (dash blue line) with analytical solution (solid red line) of the defocusing cmKdV equation (1)

4.4.2 Subcase D_2 : $r_-^l \leq r_{BCD}^*$ and $r_+^l > r_{BCD}^*$

Two genus-1 DSWs and more genus-2 DSW are produced in this case. By adjusting the parameters r_-^l and r_-^r one can control the movement styles of the two genus-1 DSWs including the case when they collide with each other, where the genus-2 DSW appears. Define two critical points $r_{D_2}^*$ and $r_{D_2}^{**}$ as follows:

- Let $r_{D_2}^*$ solve the implicit equation $v_2(r_+^r, r_+^l, r_-^l) = v_3(r_+^l, r_-^l, r_{D_2}^*, r_{D_2}^*)$ in the interval $(-\infty, r_{D_2}^{**})$, where $r_{D_2}^{**}$ can be formulated below.
- Let $r_{D_2}^{**}$ solve the implicit equation $v_2(r_+^r, r_+^l, r_-^l) = v_3(r_+^r, r_-^l, r_{D_2}^{**}, r_{D_2}^{**})$ in the interval $(-\infty, r_-^l)$.

The complete classification of case D_2 can be given by classifying the initial values r_-^l and r_-^r , which described in Table 13. Similar to Table 11, the region remarked by D_{2,g_2} also represents the genus-2 region.

The classification of solutions and region distributions for the subcases $D_{2,11}$, $D_{2,21}$, $D_{2,54}$ and $D_{2,55}$ listed in Table 13 are given in Table 14. It is seen that there are two genus-1 DSWs in each case and the rarefaction waves don't emerge here. The density

Table 13 All of possible solution cases under condition D_2

Conditions	$r_-^r < r_{D_2}^*$	$r_-^r = r_{D_2}^*$	$r_{D_2}^* < r_-^r < r_{D_2}^{**}$	$r_-^r = r_{D_2}^{**}$	$r_-^r < r_{D_2}^{**}$
$r_-^l < r_{D_2}^*$	$D_{2.11}$	Null	Null	Null	Null
$r_-^l = r_{D_2}^*$	$D_{2.21}$	Null	Null	Null	Null
$r_{D_2}^* < r_-^l < r_{D_2}^{**}$	$D_{2.g2}$	$D_{2.g2}$	$D_{2.g2}$	Null	Null
$r_-^l = r_{D_2}^{**}$	$D_{2.g2}$	$D_{2.g2}$	$D_{2.g2}$	Null	Null
$r_-^l > r_{D_2}^{**}$	$D_{2.g2}$	$D_{2.g2}$	$D_{2.g2}$	$D_{2.54}$	$D_{2.55}$

Table 14 Classification of solutions and region distributions for the subcases $D_{2.11}, D_{2.21}, D_{2.54}$ and $D_{2.55}$ listed in Table 13 under condition D_2

Cases	Regions				
	Region 1	Region 2	Region 3	Region 4	Region 5
$D_{2.11}$	Plateau	{DSW-II}	Plateau	{DSW-I}	plateau
$D_{2.21}$	Plateau	{DSW-II}	{DSW-I}	Plateau	Null
$D_{2.54}$	Plateau	{DSW-I}	{DSW-II}	Plateau	Null
$D_{2.55}$	Plateau	{DSW-I}	Plateau	{DSW-II}	Plateau

profiles are very similar to case D_1 so we don't display the Riemann invariants and the comparison of numerical simulation with Whitham modulation theory here.

4.4.3 Subcase $D_3: r_+^l < r_{BCD}^*$

Notice that the distribution of Riemann invariants in this case is symmetric with case D_1 and the density profile ρ is exactly the same as case D_1 . In fact, the symmetry of {DSW-II}, {DSW-VI}, {RW-IV}, {RW-I} in case D_3 is {DSW-I}, {DSW-VI}, {RW-VI}, {RW-II} in case D_1 , respectively. Thus we omit the whole description here for simplicity.

4.5 Case E. $r_+^r > r_+^l > r_-^r > r_-^l$

The classification of solutions under condition E is the same as that in case B . Indeed, if setting $r_{+E}^r = -r_{-B}^r, r_{+E}^l = -r_{-B}^l, r_{-E}^r = -r_{+B}^r, r_{-E}^l = -r_{+B}^l$ where subscripts B and E represent the parameters under conditions B and E , respectively, we have immediately that $r_{+B}^l > r_{+B}^r > r_{-B}^l > r_{-B}^r$, which exactly coincides with the condition in case B . Moreover, the same symmetry can also be found in Whitham velocities as follows:

$$\begin{aligned}
 v_j(-\lambda_4, -\lambda_3, -\lambda_2, -\lambda_1) &= V - (-s_1 + 2\lambda_j)(\partial \ln L / \partial \lambda_j)^{-1} \\
 &= V - (-s_1 - 2\lambda_i)(-\partial \ln L / \partial \lambda_i)^{-1} \\
 &= V - (s_1 + 2\lambda_i)(\partial \ln L / \partial \lambda_i)^{-1} \\
 &= v_i(\lambda_1, \lambda_2, \lambda_3, \lambda_4), \quad i = 5 - j.
 \end{aligned} \tag{96}$$

This proves our claim, so the detailed analysis for case E can omit for simplicity.

4.6 Case F. $r_+^r > r_-^r > r_+^l > r_-^l$

Similarly, the classification of solutions in this case is the same as that in case C . Setting $r_{+F}^r = -r_{-C}^r$, $r_{+F}^l = -r_{-C}^l$, $r_{-F}^r = -r_{+C}^r$, $r_{-F}^l = -r_{+C}^l$ yields $r_{+C}^l > r_{-C}^l > r_{+C}^r > r_{-C}^r$, which exactly coincides with the condition in case C .

5 Conclusion

The Riemann problem of the defocusing cmKdV equation has been investigated by Whitham modulation theory. The periodic solutions along with the Whitham equations in diagonal form are derived by means finite-gap integration approach. The complete classification for the general step-like initial data of the defocusing cmKdV equation have been discussed in six cases. Some new basic wave structures that do not appear in the NLS equation are found. The solution regions in the NLS equation consisted of five parts, while they can contain six regions in the defocusing cmKdV equation. The typical density profiles in each class have been compared with the direct numerical simulation with remarkable agreement.

During the analysis of the initial value problem of the defocusing cmKdV equation, an asymptotical description of the slowly modulated waves is given by solving the Whitham equations. However, the Whitham method is not the only way to investigate the asymptotics of the nonlinear integrable systems and the Riemann-Hilbert method, especially the Deift–Zhou nonlinear steepest descent approach (Deift and Zhou 1993) is a rigorous path to explore the asymptotics of various integrable systems, such as the nonlinear Schrödinger equation (Boutet de Monvel et al. 2020, 2021; Kotlyarov and Minakov 2019), KdV equation (Andreiev et al. 2016), real modified KdV equation (Grava and Minakov 2020), Camassa-Holm equation (Chang et al. 2016) and Toda lattice (Egorova et al. 2018). The results in this work will inspire further exploration of the long-time behaviors of the defocusing cmKdV equation based on Deift–Zhou nonlinear steepest descent approach (Deift and Zhou 1993).

Acknowledgements The authors gratefully thank the referees for their valuable suggestions. The work of DSW is supported by National Natural Science Foundation of China under Grant No. 11971067, the Fundamental Research Funds for the Central Universities under Grant No. 2020NTST22, and the Beijing Great Wall Talents Cultivation Program under Grant No. CIT&TCD20180325. The work of ZX is supported by Beijing outstanding talents training fund youth top individual project and Premium Funding Project for Academic Human Resources Development in Beijing Union University under Grant No. BPHR2020EZ01.

References

- Abenda, S., Grava, T.: Modulation of Camassa–Holm equation and reciprocal transformations. *Ann. Inst. Fourier (Grenoble)* **55**, 1803–1834 (2005)
- Ablowitz, M.J., Demirci, A., Ma, Y.P.: Dispersive shock waves in the Kadomtsev–Petviashvili and two dimensional Benjamin–Ono equations. *Physica D* **333**, 84–98 (2016)
- Ablowitz, M.J., Cole, J.T., Rumanov, I.: Whitham equations and phase shifts for the Korteweg–de Vries equation. *Proc. R. Soc. A* **476**, 20200300 (2020)
- Andreiev, K., Egorova, I., Lange, T.L., Teschl, G.: Rarefaction waves of the Korteweg–de Vries equation via nonlinear steepest descent. *J. Differ. Equ.* **261**(10), 5371–5410 (2016)
- Belokolos, E.D., Bobenko, A.I., Enolski, V.Z., Its, A.R., Matveev, V.B.: *Algebro-Geometric Approach to Nonlinear Integrable Equations*. Springer, New York (1994)
- Boutet de Monvel, A., Lenells, J., Shepelsky, D.: The focusing NLS equation with step-like oscillating background: the genus 3 sector. [arXiv:2005.02822](https://arxiv.org/abs/2005.02822) (2020)
- Boutet de Monvel, A., Lenells, J., Shepelsky, D.: The focusing NLS equation with step-like oscillating background: scenarios of long-time asymptotics. *Commun. Math. Phys.* **383**, 893–952 (2021)
- Bridges, T.J., Ratliff, D.J.: Nonlinear theory for coalescing characteristics in multiphase Whitham modulation theory. *J. Nonlinear Sci.* **31**, 7 (2021)
- Chang, C.H., Yu, C.H., Sheu, T.W.: Long-time asymptotic solution structure of Camassa–Holm equation subject to an initial condition with non-zero reflection coefficient of the scattering data. *J. Math. Phys.* **57**, 103508 (2016)
- Congy, T., El, G.A., Hoefler, M.A., Shearer, M.: Nonlinear Schrödinger equations and the universal description of dispersive shock wave structure. *Stud. Appl. Math.* **142**, 241–268 (2019)
- Deift, P., Zhou, X.: A steepest descent method for oscillatory Riemann–Hilbert problems. Asymptotics for the MKdV equation. *Ann. Math.* **137**(2), 295–368 (1993)
- Dubrovin, B.A., Novikov, S.P.: Hydrodynamics of weakly deformed soliton lattices. Differential geometry and Hamiltonian theory. *Russ. Math. Surv.* **44**, 35–124 (1989)
- Egorova, I., Michor, J., Teschl, G.: Long-time asymptotics for the toda shock problem: non-overlapping spectra. *J. Math. Phys. Anal. Geom.* **14**(4), 406–451 (2018)
- El, G.A., Geogjaev, V.V., Gurevich, A.V., Krylov, A.L.: Decay of an initial discontinuity in the defocusing NLS hydrodynamics. *Physica D* **87**, 186–192 (1995)
- Engquist, B., Lötstedt, P., Sjögreen, B.: Nonlinear filters for efficient shock computation. *Math. Comp.* **52**, 509–537 (1989)
- Flaschka, H., Forest, M.G., McLaughlin, D.W.: Multiphase averaging and the inverse spectral solution of the Korteweg–de Vries equation. *Commun. Pure Appl. Math.* **33**, 739–784 (1980)
- Grava, T., Klein, C.: Numerical solution of the small dispersion limit of Korteweg de Vries and Whitham equations. *Commun. Pure Appl. Math.* **60**(11), 1623–1664 (2007)
- Grava, T., Minakov, A.: On the long-time asymptotic behavior of the modified Korteweg–de Vries equation with step-like initial data. *SIAM J. Math. Anal.* **52**(6), 5892–5993 (2020)
- Gurevich, A.V., Pitaevskii, L.P.: Nonstationary structure of a collisionless shock wave, *Sov. Phys. JETP* **38**, 291–297 (translation from Russian of A.V. Gurevich and L.P. Pitaevskii, *Zh. Eksp. Teor. Fiz.* **65**, 590–604 (1973)) (1974)
- Hoefler, M.A.: Shock waves in dispersive Eulerian fluids. *J. Nonlinear Sci.* **24**, 525–577 (2014)
- Its, A.R., Kotlyarov, V.P.: Explicit formulas for solutions of the Schrödinger nonlinear equation. *Doklady Akad.Nauk Ukrainian SSR, ser. A* **10**, 965–968 (English translation is available at [arXiv:1401.4445](https://arxiv.org/abs/1401.4445)) (1976)
- Ivanov, S.K., Kamchatnov, A.M.: Riemann problem for the photon fluid: self-steepening effects. *Phys. Rev. A* **96**, 053844 (2017)
- Ivanov, S.K., Kamchatnov, A.M., Congy, T., Pavloff, N.: Solution of the Riemann problem for polarization waves in a two-component Bose–Einstein condensate. *Phys. Rev. E* **96**, 062202 (2017)
- Kamchatnov, A.M.: Whitham equations in the AKNS scheme. *Phys. Lett. A* **186**, 387–390 (1994)
- Kamchatnov, A.M.: New approach to periodic solutions of integrable equations and nonlinear theory of modulational instability. *Phys. Rep.* **286**, 199–270 (1997)
- Kamchatnov, A.M.: *Nonlinear Periodic Waves and Their Modulations: An Introductory Course*. World Scientific Publishing, Singapore (2000)
- Kamchatnov, A.M., Kuo, Y.H., Lin, T.C., Horng, T.L., Gou, S.C., Clift, R., El, G.A., Grimshaw, R.H.J.: Undular bore theory for the Gardner equation. *Phys. Rev. E* **86**, 036605 (2012)

- Kodama, Y., Pierce, V.U., Tian, F.R.: On the Whitham equations for the defocusing complex modified KdV equation. *SIAM J. Math. Anal.* **40**(5), 1750–1782 (2008)
- Kong, L.Q., Wang, L., Wang, D.S., Dai, C.Q., Wen, X.Y., Xu, L.: Evolution of initial discontinuity for the defocusing complex modified KdV equation. *Nonlinear Dyn.* **98**, 691–702 (2019)
- Kotlyarov, V.P.: Periodic problem for the Schrödinger nonlinear equation. *Voprosy matematicheskoi fiziki i funkcionalnogo analiza, Naukova Dumka, Kiev* **1**, 121–131 (English translation is available at [arXiv:1401.4445](https://arxiv.org/abs/1401.4445)) (1976)
- Kotlyarov, V., Minakov, A.: Dispersive shock wave, generalized Laguerre polynomials, and asymptotic solitons of the focusing nonlinear Schrödinger equation. *J. Math. Phys.* **60**(12), 123501 (2019)
- Lax, P., Levermore, C.: The small dispersion limit of the Korteweg-De Vries equation. *Commun. Pure Appl. Math.* **36**(3), 253–290 (1983)
- Luke, J.C.: A perturbation method for nonlinear dispersive wave problems. *Proc. R. Soc. Lond. Ser. A Math. Phys.* **292**, 403–412 (1966)
- Pierce, V.U., Tian, F.R.: Self-similar solutions of the non-strictly hyperbolic Whitham equations for the KdV hierarchy. *Dyn. Partial Differ. Equ.* **4**, 263–282 (2007)
- Tian, F.R., Ye, J.: On the Whitham equations for the semiclassical limit of the defocusing nonlinear Schrödinger equation. *Commun. Pure Appl. Math.* **52**(6), 655–692 (1999)
- Whitham, G.B.: Nonlinear dispersive waves. *Proc. R. Soc. Lond. Ser. A* **283**, 238–261 (1965)

Publisher's Note Springer Nature remains neutral with regard to jurisdictional claims in published maps and institutional affiliations.